

2000

# The enhancement of IrMn spin-valve performance by introduction of oxygen layers

Hung-Chen Chang  
*San Jose State University*

Follow this and additional works at: [https://scholarworks.sjsu.edu/etd\\_theses](https://scholarworks.sjsu.edu/etd_theses)

---

## Recommended Citation

Chang, Hung-Chen, "The enhancement of IrMn spin-valve performance by introduction of oxygen layers" (2000). *Master's Theses*. 2039.

DOI: <https://doi.org/10.31979/etd.xpr5-4dr>

[https://scholarworks.sjsu.edu/etd\\_theses/2039](https://scholarworks.sjsu.edu/etd_theses/2039)

This Thesis is brought to you for free and open access by the Master's Theses and Graduate Research at SJSU ScholarWorks. It has been accepted for inclusion in Master's Theses by an authorized administrator of SJSU ScholarWorks. For more information, please contact [scholarworks@sjsu.edu](mailto:scholarworks@sjsu.edu).

## **INFORMATION TO USERS**

**This manuscript has been reproduced from the microfilm master. UMI films the text directly from the original or copy submitted. Thus, some thesis and dissertation copies are in typewriter face, while others may be from any type of computer printer.**

**The quality of this reproduction is dependent upon the quality of the copy submitted. Broken or indistinct print, colored or poor quality illustrations and photographs, print bleedthrough, substandard margins, and improper alignment can adversely affect reproduction.**

**In the unlikely event that the author did not send UMI a complete manuscript and there are missing pages, these will be noted. Also, if unauthorized copyright material had to be removed, a note will indicate the deletion.**

**Oversize materials (e.g., maps, drawings, charts) are reproduced by sectioning the original, beginning at the upper left-hand corner and continuing from left to right in equal sections with small overlaps.**

**Photographs included in the original manuscript have been reproduced xerographically in this copy. Higher quality 6" x 9" black and white photographic prints are available for any photographs or illustrations appearing in this copy for an additional charge. Contact UMI directly to order.**

**Bell & Howell Information and Learning  
300 North Zeeb Road, Ann Arbor, MI 48106-1346 USA**

**UMI<sup>®</sup>**  
**800-521-0600**



**THE ENHANCEMENT OF IrMn SPIN-VALVE PERFORMANCE BY  
INTRODUCTION OF OXYGEN LAYERS**

A Thesis Proposal

Presented to

The Faculty of the Department of Chemical and Materials Engineering

San Jose State University

In Partial Fulfillment

of the Requirements for the Degree

Master of Science

By

Hung-Chen Chang

July 2000

**UMI Number: 1400652**

**Copyright 2000 by  
Chang, Hung-Chen**

**All rights reserved.**

**UMI<sup>®</sup>**

---

**UMI Microform 1400652**

**Copyright 2000 by Bell & Howell Information and Learning Company.  
All rights reserved. This microform edition is protected against  
unauthorized copying under Title 17, United States Code.**

---

**Bell & Howell Information and Learning Company  
300 North Zeeb Road  
P.O. Box 1346  
Ann Arbor, MI 48106-1346**

© 2000

Hung-Chen Chang

ALL RIGHTS RESERVED

APPROVED FOR THE DEPARTMENT OF  
CHEMICAL AND MATERIALS ENGINEERING

  
\_\_\_\_\_

Dr. Emily L. Allen

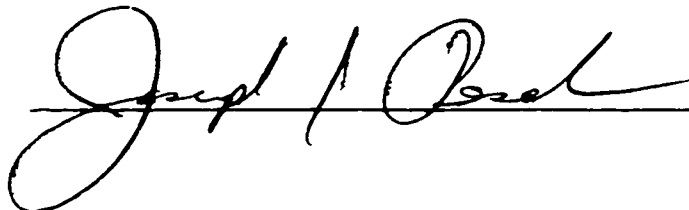
  
\_\_\_\_\_

Dr. Richard L. Comstock

  
\_\_\_\_\_

Dr. Wen-Yuang Lee, IBM Almaden Research Center

APPROVED FOR THE UNIVERSITY

  
\_\_\_\_\_

## **Abstract**

### **THE ENHANCEMENT OF IrMn SPIN-VALVE PERFORMANCE BY INTRODUCTION OF OXYGEN LAYERS**

by Hung-Chen Chang

The oxygen exposure effect in single (bottom) and dual IrMn spin-valves is reported. The oxygen exposure position in the single spin-valve was within the pinned layer. Different oxygen exposure dosages were studied in single spin-valve. The exposure in the dual spin-valve was studied in different positions: the bottom pinned, bottom spacer, top spacer, and top pinned layers. The sheet resistance and interlayer coupling field of both single and dual spin-valves were reduced by the exposure to oxygen. These results indicate that a smooth interface as a result of the oxygen exposure was formed. This smooth interface enhances the specular electron scattering. Therefore, the GMR effect of both single and dual spin-valves was enhanced significantly if a best oxygen exposure dosage and an optimal oxygen exposure position were used. The best GMR ratio of single and dual spin-valves was 13.1% and 18.9%, respectively.



## **Acknowledgments**

After spending one year on this study, I would like to thank the following people. First, I would like to thank Dr. Emily Allen, my thesis advisor, for her helpful advisement and effort in reviewing the drafts. Second, I would like to thank Dr. Wen-Yuang Lee for his invaluable guidance and support to me on experiments. Third, I would like to thank Dr. Richard L. Comstock for being kindly as my reading committee member. Without their help, I would not have been able to complete this thesis.

This thesis has been funded by National Science Foundation Grant [DMR#9502290] and sponsored by IBM Almaden Research Center.

## **Table of Contents**

<b>Chapter</b>	<b>Page</b>
<b>1. Introduction</b>	1
1.1 Background	1
1.2 GMR Effect	1
1.3 Spin-Valve	2
1.4 Electrons Scattering in Spin-Valve	3
1.5 Magnetic Properties Requirements in Spin-Valve	6
1.5.1 GMR Ratio	6
1.5.2 Pinning Field	7
1.5.3 Interlayer Coupling Field	8
1.5.4 Coercivity of Free Layer	9
1.6 Other Requirements in Spin-Valve	10
1.7 Thesis Objectives	10
<b>2. Literature Review</b>	11
2.1 Purpose of Review	11
2.2 Different Types of Spin-Valve	12
2.3 Pinning Field, $H_{UA}$	13
2.3.1 Interfacial Exchange Coupling Energy	13
2.3.2 Crystal Structure	14
2.3.3 Composition	15

2.3.4 Thermal Stability	15
2.4 Interlayer Coupling Field, $H_f$	16
2.5 Thin Film Resistance	18
2.6 The Effect of Under Layer	20
2.7 Thesis Orientation	22
<b>3. Experimental Procedures</b>	<b>23</b>
3.1 Experimental Plan	23
3.2 Sample Preparation	24
3.2.1 Substrate Cleaning	24
3.2.2 Thin Film Deposition	24
3.2.3 Annealing	26
3.3 Sample Measurement	26
3.3.1 VSM Measurement	26
3.3.2 B-H Loop Tracer Measurement	27
3.3.3 Sheet Resistance Measurement	28
3.4 Experiment I	30
3.5 Experiment II	30
3.6 Experiment III	32
3.7 Experiment IV	33
3.8 Experiment V	33
3.9 Reproducibility of Samples	36

<b>4. Results and Discussion</b>	<b>39</b>
4.1 The Effect of the Oxygen Exposure on GMR Ratio	39
4.2 The Effect of the Oxygen Exposure on Sheet Resistance	42
4.3 The Effect of the Oxygen Exposure on Interlayer Coupling Field	43
4.4 Discussion of Sheet Resistance and $H_f$	47
4.5 Shift of Hysteresis Loop in Dual Spin-Valve	48
<b>5. Conclusions</b>	<b>50</b>
5.1 Summary	51
5.2 Suggestions for Future Study	52

## **List of Tables**

<b>Table</b>	<b>Page</b>
1. Some antiferromagnetic materials' blocking temperature	9
2. Summary of different AFM materials	14
3. The experimental samples of the Experiment I	31
4. The experimental samples of the Experiment II	32
5. The experimental samples of the Experiment III	34
6. The experimental samples of the Experiment IV.	35
7. The experimental plan of the Experiment V.	38

## List of Figures

<b>Figure</b>	<b>Page</b>
1. Schematic of (a) magnetic/nonmagnetic superlattice structure, (b) single spin-valves structure (bottom and top spin-valves), (C) dual spin-valve.	4
2. Atomic magnetic moments of (a) ferromagnet and (b) antiferromagnet.	4
3. A schematic of electron scattering situation in single spin-valve.	6
4. Exchange across a FM-AFM interface.	8
5. Schematic view of possible rotating of magnetic dipole moments in antiferromagnet and ferromagnet.	14
6. Dependence of $H_{ua}$ on IrMn composition for Zr/IrMn/NiFe/Zr/Si.	16
7. Normalized pinning fields vs. temperature for NiMn, FeMn, IrMn, and NiO spin-valves.	17
8. An illustration of orange peel coupling.	18
9. Illustration of specular electron scattering increase the electron mean free path.	19
10. A schematic of how oxygen smoothing the interface of cobalt film.	19
11. (a) $H_{UA}$ and (b) Intensity of (1110) diffraction peaks vs. Zr layer thickness.	21
12. A schematic plot of DC magnetron sputtering system.	25
13. VSM measurement-hysteresis loop.	27

14. (a) Magnetization curve of free layer measurement; (b) the GMR ratio measurement.	29
15. A schematic of CoFe single layer deposition; (a) the first step of CoFe deposition; (b) the second step of CoFe deposition.	31
16. A schematic plot of multilayer structure in Experiment II.	32
17. The bottom spin-valve structure in Experiment III.	34
18. The bottom spin-valve structure in Experiment IV.	35
19. A schematic plot of dual spin-valve structure in Experiment V.	37
20. The GMR ratio of bottom spin-valve with different O <sub>2</sub> exposure positions and dosages.	40
21. The GMR ratio of bottom spin-valve with different Cu spacer layer thickness.	40
22. The GMR ratio of dual spin-valve with different oxygen exposure positions.	41
23. The pinning field of bottom spin-valve with O <sub>2</sub> exposure.	42
24. The sheet resistance of the single Co <sub>90</sub> Fe <sub>10</sub> layer with and without oxygen exposure.	44
25. The sheet resistance of the multilayer structure.	44
26. The sheet resistance of bottom spin-valve with different O <sub>2</sub> exposure positions and dosages.	45
27. The effect of the oxygen exposure effect on interlayer coupling field, H <sub>f</sub> .	45

28. The $H_f$ vs. the Cu spacer layer thickness.	46
29. The $H_f$ change with the different oxygen exposure positions in dual spin-valve.	46
30. The structure of different pinned layer thickness dual spin-valve.	49
31. The VSM measurement of the different pinned layer thickness dual spin-valve.	50



# Chapter 1

## Introduction

### 1.1 Background

The change in electrical resistance of a material in response to a magnetic field is called magnetoresistance (MR). In 1988, Baibich and his colleagues<sup>(1)</sup> reported that a large change of magnetoresistance was discovered in  $(\text{Fe/Cr})_n$  multilayer ultra thin film. Because, in this thin film, the MR effect reached about 80% at 4.2K, it was immediately labeled as “giant magnetoresistance (GMR)” effect<sup>(1)</sup>. Later on, the concept of using GMR effect for magnetic storage was proposed. In late 1997, the industry’s first hard disk drive (HDD) product using a GMR read head was announced by IBM. By the year 2001, it is expected that a commercial HDD will require areal densities of 10 Gbits/in<sup>2</sup>. Therefore, many studies are being devoted to developing a higher sensitivity reading head for this application.

### 1.2 GMR Effect

The multilayer thin film, Figure 1(a), in Baibich’s study was constructed by depositing consecutive ferromagnetic and non-magnetic layers. In a later study<sup>(2)</sup>, it was reported that two requirements, as shown below, must be met to make the GMR effect appear.

1. The magnetization vector in adjacent magnetic layers (Figure 1(a)) must be free to rotate.

2. The multilayer film must be thinner than the mean free path of an electron in the multilayer film.

The GMR is attributed to the spin dependent conduction properties of the ferromagnetic metals. The magnitude of the GMR effect can be evaluated by the GMR ratio. The definition of the GMR ratio is given in Equation 1.

$$\text{GMR Ratio} = [R(H_{\text{max}}) - R_0] / R_0 = \Delta R/R_0 \quad (\text{Eq. 1})$$

where  $R_0$  is the resistance of the GMR film when it is in magnetic saturation along the easy axis, and  $R(H_{\text{max}})$  is the resistance at maximum applied field. Because the films' magnetic saturation fields in Baibich's study were too high for real applications, it became desirable to lower the magnetic saturation field, while maintaining a large  $\Delta R$ .

### 1.3 Spin-Valve

In 1991, Dieny and colleagues reported very large GMR effects in sandwiches consisting of two uncoupled ferromagnetic layers with in-plane anisotropy separated by a nonmagnetic metal<sup>(2)</sup>. This study showed that one of the ferromagnetic magnetization vectors was free to rotate, and the other one (the pinned layer) was constrained by the antiferromagnetic pinning layer, as shown in Figure 1(b). Because of the operation of the film, the sandwich structure was named a "spin-valve". In addition, the free rotation of the ferromagnetic magnetization could be done under a low magnetic field. Therefore, this brought the GMR effect into applications.

Spin-valves include single and dual spin-valves. There are two kinds of single spin-valves: bottom and top pinned spin-valve. A typical single bottom spin-valve structure consists of ferromagnetic (FM) / nonmagnetic (NM) / ferromagnetic /

antiferromagnetic (AFM) layers, show in Figure 1(b) (left figure). In Figure 1(b) left, the top first layer is called the free layer. The material for this layer is ferromagnet, which is usually a permalloy (NiFe) thin film. The second, nonmagnetic layer, is called the spacer layer, and the material is usually Cu. The third layer is called the pinned layer. This layer is a ferromagnetic layer. The fourth layer is called the pinning layer, and it is made of an antiferromagnetic material. Because the pinned layer of this spin-valve is below the free layer, it is called a bottom spin-valve. The other type of spin-valve has the pinned layer above the free layer. It is, therefore, called a top spin-valve, Figure 1(b) right figure.

A schematic of the dual (or symmetric) spin-valve structure is shown in Figure 1(c). Because this structure has pinned layers on both sides of the free layer, it is called a dual spin-valve. A dual spin-valve has a significantly longer electron mean free path in its seven-film structure than single spin-valves have when the magnetization vectors of the two ferromagnetic layers are in parallel alignment. When the magnetization vectors of the two ferromagnetic layers are in antiparallel alignment, both single and dual spin-valves experience a shorter mean free path. Therefore, it is expected that a dual spin-valve will have a higher GMR ratio than a single spin-valve.

#### **1.4 Electron Scattering in Spin-Valve**

A ferromagnet, Figure 2(a)<sup>(3)</sup>, is a material in which adjacent magnetic dipole moments tend to line up in the same direction. An antiferromagnet, Figure 2(b)<sup>(3)</sup>, is a material in which adjacent magnetic dipole moments tend to line up in the opposite directions, and there is no net magnetic moment in the material.

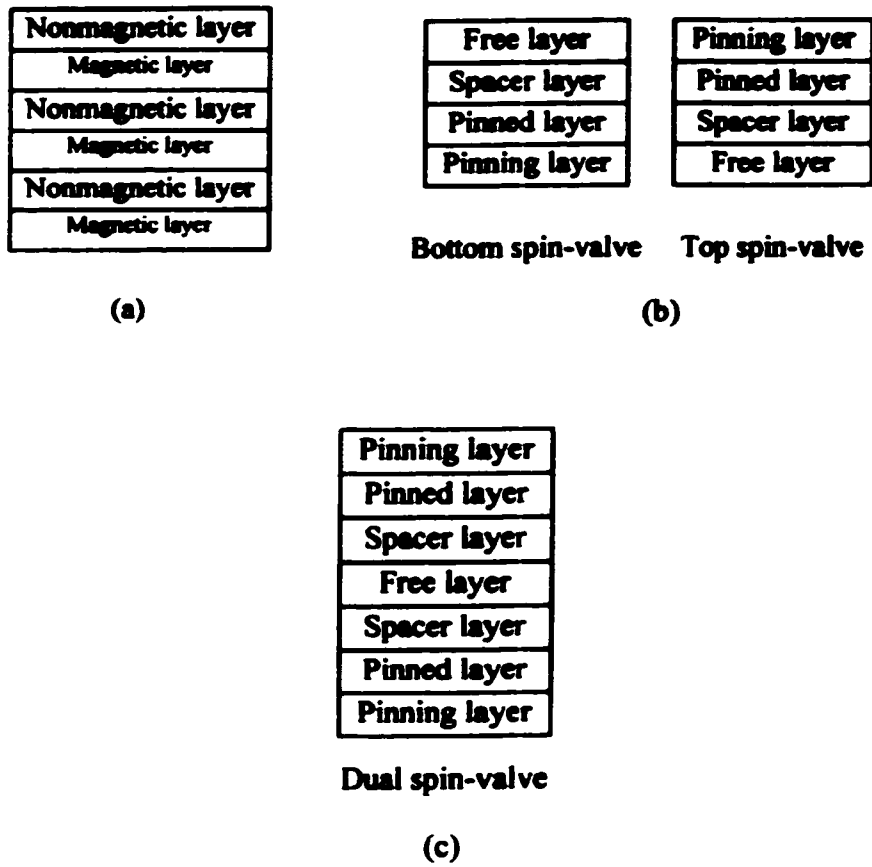


Figure 1. Schematic of (a) magnetic/nonmagnetic superlattice structure, (b) single spin-valves structure (bottom and top spin-valves), (c) dual spin-valve.

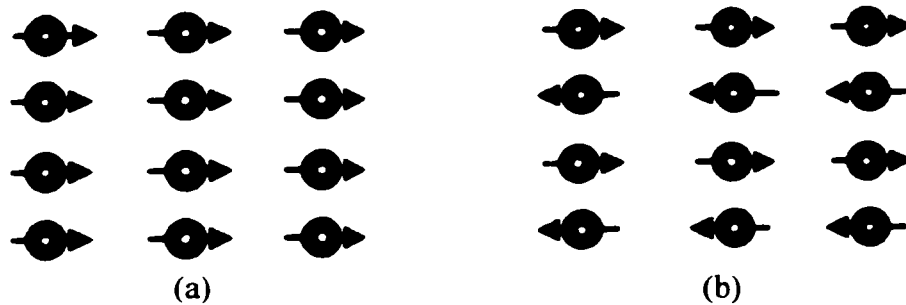


Figure 2. Atomic magnetic moments of (a) ferromagnet and (b) antiferromagnet<sup>(3)</sup>.

In a spin-valve multilayer film, electrical resistance is related to the relative magnetization angle between two ferromagnetic layers. A simple model that explains this phenomenon is shown in Figure 3. Conduction electrons that flow in magnetic films can be classified into those with parallel spin and those with antiparallel spin relative to the local magnetization. The electrons with parallel spin have a long mean free path and experience very little scattering. Therefore, the resistance is relatively small. On the contrary, the electrons with antiparallel spin have shorter mean free paths and experience more scattering. The resistance is, consequently, relatively large. In Figure 3(a), electrons of both spins are highly scattered because the two FM layers have opposite magnetization vectors. The result is the total resistance of the multilayer film increases. In Figure 3(b), the magnetization of the free layer is parallel to that of the pinned layer. The electrons with spin parallel to the magnetization direction are not scattered too many times and provide a low-resistance path. The other electrons with antiparallel spin are highly scattered and produce high resistance. Because the resistance will be shunted by the low resistance electrons, the result is the trilayer film experiences relatively low resistance. This is what creates the GMR effect, in which the electrical resistance has a large change in response to a magnetic field.

The spin-valve reading sensor was developed by using the change of resistance of a spin-valve film in response to the magnetization of the media. An electrical current applied to the reading head generates a varying voltage signal due to the changes in resistance of the reading head, which is controlled by the magnetic field of media.

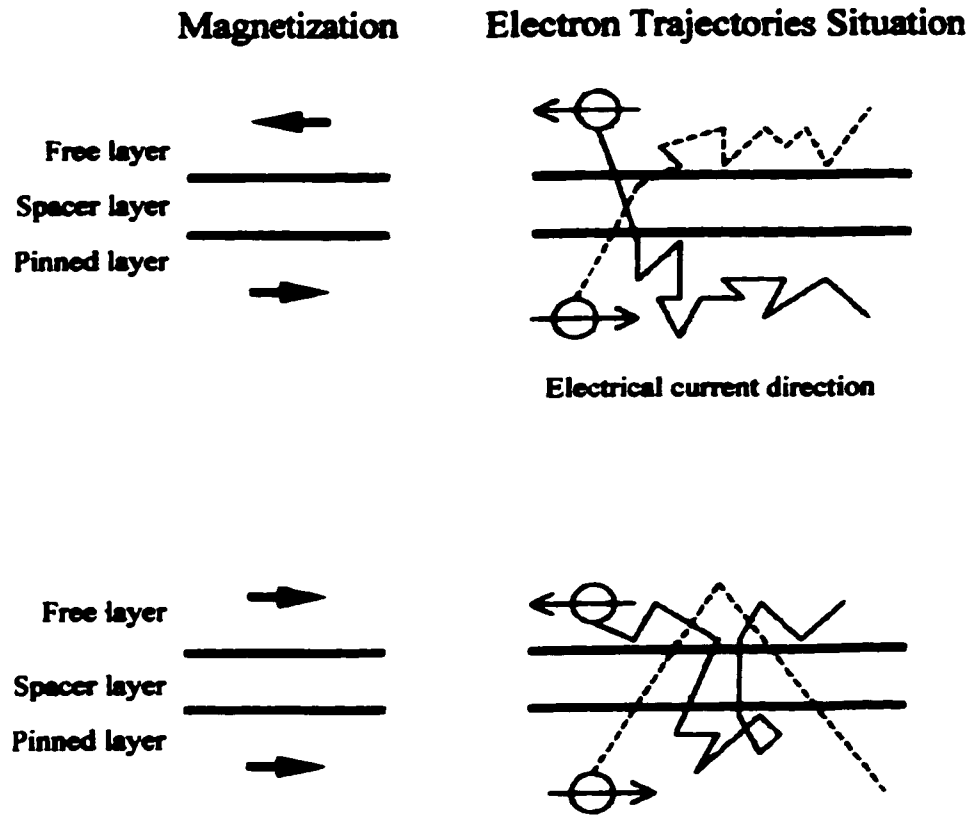


Figure 3. A schematic of electron scattering situation in a single spin-valve.

## 1.5 Magnetic Properties Requirements in Spin-Valve

For the best application of the spin-valve sensor, high GMR ratio, low interlayer coupling field between pinned and free layers ( $H_f$ ), large pinning field ( $H_{UA}$ ), and low coercivity of the free layer ( $H_{cf}$ ), are required.

### 1.5.1 GMR Ratio

GMR ratio, as shown in Equation 1, is related to the total resistance change and the resistance of the GMR film. If the GMR ratio is large, the varying voltage in the reading head is also large. This means a clear signal output. In addition, under the same

signal output the bit in the media can be smaller. Therefore, a large GMR ratio is preferred in applications. For the typical media areal density of 40 GB/in<sup>2</sup> and 80 GB/in<sup>2</sup> application, the GMR ratio required is 12% and 15%, respectively.

### **1.5.2 Pinning Field**

The tendency for neighboring atomic dipoles to line up parallel or antiparallel to each other is called exchange coupling<sup>(3)</sup>. Figure 4 shows an example of exchange coupling between these two layers, and shows a simple explanation of how the AFM layer (pinning layer) pins the FM layer. The first layer of atomic dipoles of the AFM material aligns with the lowest layer of the atomic dipoles of the FM material. Because of the antiferromagnetic exchange coupling within the AFM layer, the second layer of the atomic dipoles of the AFM material aligns opposite to the direction of the first layer. Under this situation, a higher magnetic field is needed to change the magnetic direction of the FM layer. The magnetic direction of the FM layer is then pinned by the AFM layer. The magnetic field required to reverse the direction of the pinned layer is called the pinning field ( $H_{UA}$ ).

It has been established<sup>(4)</sup> that the pinning field is inversely proportional to the thickness of the pinned layer. The value of the pinning field indicates how well the magnetic moment of the pinned layer is pinned by the pinning layer. The higher the value of  $H_{UA}$ , the stronger is the pinning. If the moment of the layer is pinned well, the free layer and the pinned layer can have a better antiparallel magnetic moment state while in operation and provide a better GMR ratio.

The value of  $H_{UA}$  can be affected by the presence of an under layer. The under

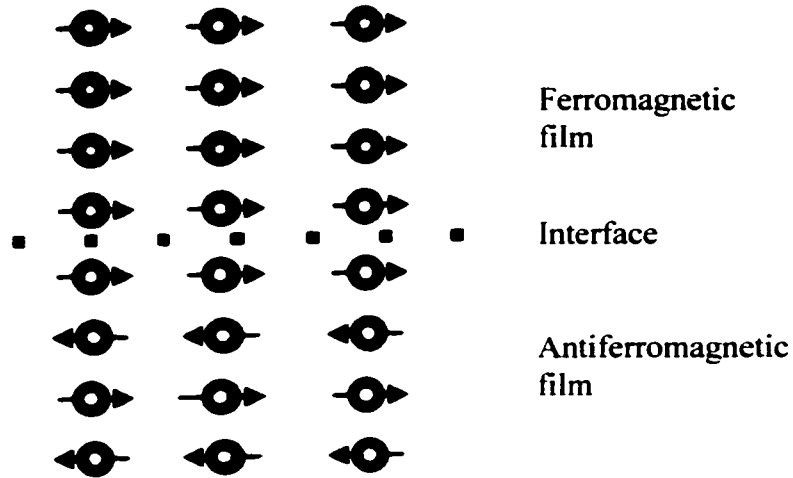


Figure 4. Exchange across a FM-AFM interface.

layer can help the AFM layer to grow with a smoother interface and in a desired texture, so that the AFM layer can pin the FM layer more strongly.

The pinning field decreases with increasing temperature. When the blocking temperature is reached, the pinning phenomenon disappears. The disappearance of pinning is related to the loss of magnetic order in the AFM layer due to thermal excitation<sup>(4)</sup>. Because the operational temperature of a HDD drive is usually about 100°C, a high blocking temperature is required to keep the pinning field existing while the HDD is in operation. The blocking temperature is related to the properties of antiferromagnetic layer materials. Different blocking temperatures of AFM materials are listed in Table 1.

### 1.5.3 Interlayer Coupling Field

The interlayer coupling field ( $H_I$ ) is due to the magnetostatic interaction between



the two ferromagnetic layers, which are separated by a nonmagnetic spacer layer. It was found that the interlayer coupling field increases as the spacer layer decreases<sup>(5)</sup>. In HDD applications, a small interlayer coupling field, less than 10 Oe, is required, so the spacer layer thickness must be thicker than a certain value to have a small  $H_f$ . Unfortunately, there is a conflict here. The material for the spacer layer is usually Cu, which has low resistivity. The thicker the spacer, the lower the resistance of the spin-valve film. This causes a reduction of the GMR ratio. Therefore, there is an optimal thickness for the spacer layer.

#### 1.5.4 Coercivity of Free Layer

In the free layer, the materials to be used need to be magnetically soft. A typical value of free layer coercivity ( $H_{cf}$ ) needs to be smaller than 10 Oe for applications. The main reason is the sensor's sensitivity. If a high coercivity material were to be used, there would be less or no change in the magnetic moment of the free layer under small magnetic fields. Hence, the GMR ratio would be small, and the overall sensitivity would be poor.

Table 1. Some antiferromagnetic materials' blocking temperature.

Materials	Blocking Temp.
Ir-Mn	~250°C
Fe-Mn	~150°C
Ni-Mn	~350°C
Pt-Mn	~400°C

## **1.6 Other Requirements in Spin-Valve**

Interfacial roughness in the spin-valve multilayer structure affects the interlayer coupling field and GMR ratio. Studies<sup>(6-12)</sup> show that the introduction of an under layer or a surfactant can reduce the interlayer coupling field and increase the GMR ratio. This is because both a surfactant and an under layer can provide a smooth interface between layers which can reduce surface scattering<sup>(6-8)</sup> and can reduce the interdiffusion between the pinned and the spacer layers<sup>(4)</sup>. Therefore, the interlayer coupling field and GMR ratio are improved. Different under layer materials (such as Ta and Cu) and different surfactants (such as Pb and O) were studied under different conditions<sup>(6-12)</sup>. Details will be discussed in Chapter 2.

## **1.7 Thesis Objectives**

This thesis investigated the use of an oxygen surfactant layer to improve spin-valve performance. Specially, the effect of oxygen exposure position and dosage in single (bottom) and dual spin-valves was determined. The objective was to achieve the largest GMR ratio possible in single and dual spin-valves. The materials that were investigated were  $\text{Co}_{90}\text{Fe}_{10}$  and  $\text{Co}_{80}\text{Fe}_{20}$  for the free and pinned layers,  $\text{Ir}_{30}\text{Mn}_{70}$  for the AFM layer, Cu for the spacer and under layer, and Ta for under layer and overcoat. The thickness of each layer in the spin-valves was optimized, and the roughness of the interface in spin-valves was smoothed by oxygen surfactant. It was found that a GMR ratio of 18.9% could be reached in a dual spin-valve and 13.1% could be reached in a bottom spin-valve.

## Chapter 2

### Literature Review

#### 2.1 Purpose of Review

The change in electrical resistance of a material in response to a magnetic field is called magnetoresistance (MR). The GMR effect can be evaluated by the GMR ratio, which is equal to the total resistance change divided by the resistance of the material when it is in magnetic saturation along its easy axis (Equation 1). In 1988, a large MR ratio, 80%, was reported. It was labeled giant magnetoresistance (GMR). However, the pinning field in this study was too high to be used in a HDD reading head. The GMR effect was first brought into application by the use of a spin-valve structure. The fundamental spin-valve structure consists of pinning/pinned/spacer/free layers. In this structure, the GMR ratio, the pinning field ( $H_{UA}$ ), and the interlayer coupling field ( $H_f$ ) are the three most important parameters.

In order to understand the studies of pinning properties that have been done and that need to be done, the literature review tried to answer the following questions:

1. What are the differences between single and dual spin-valves?
2. What are the pinning fields in different material systems?
3. What controls the pinning field?
4. How does annealing affect spin-valves?
5. What are the relationships between the magnetic properties and the layer thickness?

6. How does the interfacial roughness in spin-valve multilayer film affect the electron scattering?
7. How does the O<sub>2</sub> affect the interfacial roughness?
8. How does the under layer affect the spin-valve multilayer film?

Section 2.2 reviewed the single and dual spin-valve related articles. Section 2.3 reviews articles that report pinning field related topics. Topics relating to the interlayer coupling field are reviewed in Section 2.4. Articles relating to the interface roughness are discussed in Section 2.5. Section 2.6 reviews the articles that discuss the under layer. A summary of the literature review is given in Section 2.7.

## **2.2 Different Types of Spin-Valve**

Fundamental concepts of spin-valves, including conditions for appearance of the GMR effect, the mechanism of the GMR, and the operation of spin-valves, are given in References 13 and 14. Detailed spin-valve structures and how they operate are reviewed in References 2, 4, 15 and 16.

The spin-valve structure can be separated into three basic types: bottom spin-valve, top spin-valve, and dual spin-valve. The basic concepts of the spin-valve were reported in Chapter 1, and the schematic of these spin-valves was given in Figure 1(b) and 1(c). The top spin-valve has the pinning layer above the free layer, and the pinning layer is the most outer layer in the spin-valve. If the AFM material used in this layer is sensitive to corrosion, and also, if the AFM layer is not well protected, it may cause problems during operation since the reading sensor is very close to the surface of the media. Because of that, the bottom and dual spin valves were studied in this thesis.

## 2.3 Pinning Field, $H_{UA}$

Many discussions of topics related to the pinning field were found in the literature<sup>(4, 10, 17, 30)</sup>. These studies focused on the interfacial exchange coupling energy, crystal structure, composition, and thermal stability of AFM materials.

### 2.3.1 Interfacial Exchange Coupling Energy

The pinning field ( $H_{UA}$ ) is generally expressed by Equation 2<sup>(10)</sup>.

$$H_{UA} = J / (M_s * t) \quad (\text{Eq. 2})$$

where  $J$  is interfacial exchange coupling energy,  $M_s$  is the saturation magnetization of the pinned ferromagnetic film, and  $t$  is the thickness of the pinned ferromagnetic film. Different AFM materials, including IrMn, FeMn, NiO, and CrMnPt, have been studied<sup>(17-27)</sup>. Table 2 shows the interfacial exchange coupling energy of different AFM/FM combinations.

The mechanism of AFM/FM exchange coupling is not fully understood. Figure 5<sup>(17)</sup> shows a schematic view of the possible rotation of magnetic dipole moments in AFM and FM in response to an applied magnetic field. Because it is believed that the pinning field is related to the spin distribution and arrangement at the interface of the AFM and FM layers, the larger the interfacial exchange coupling energy, the larger the resulting pinning field. In addition, since the magnetization vector of the pinned (FM) layer is pinned by the AFM layer, an applied magnetic field  $H$ , as shown in Figure 5(b), is required to rotate the magnetization vector of the FM layer. Therefore, a shift of the hysteresis loop of the AFM/FM system can be observed. From the shift of the hysteresis loop, the pinning field can be measured.

Table 2. Summary of different AFM materials

AFM/FM Material	J (erg/cm <sup>2</sup> )	AFM desired texture	Blocking Temperature	Annealing requirement	References
IrMn/CoFe	0.192	FCC in (111)	~250°C	not required	21
FeMn/NiFe	0.13	FCC in (111)	~150°C	not required	22
NiO/NiFe	0.059	FCC in (111)	~230°C	not required	4, 23
CrMnPt/NiFe	0.15	BCC	~230°C	required	14, 24
NiMn/NiFe		FCT	~380°C	required	19

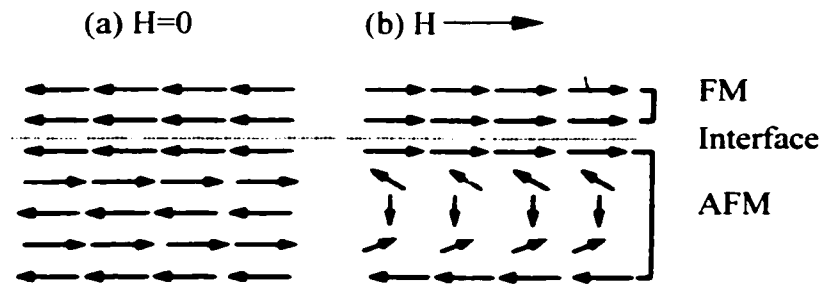


Figure 5. Schematic view of possible rotation of magnetic dipole moments in antiferromagnet and ferromagnet: (a) without applied field; (b) with an applied field<sup>(17)</sup>.

### 2.3.2 Crystal Structure

The film structure of the AFM material is an important issue in determining the pinning field. In Mn-based alloys, the alloys with  $\alpha$ -Mn do not have antiferromagnetic properties at room temperature (RT). Only the Mn-based alloys with  $\gamma$ -Mn structure show antiferromagnetic properties at RT. An example is NiMn<sup>(18)</sup>, which has a face-centered-cubic structure. In this structure, NiMn is not antiferromagnetic. However, if the structure of NiMn has a face-centered-tetragonal structure, NiMn is antiferromagnetic and can provide exchange coupling between NiMn (pinning layer) and FM pinned layer.

In general, thermal treatment (usually annealing) is required for some AFM materials because it can induce a phase transition to form a desired film structure for AFM layer, so that the AFM layer can provide pinning ability to pinned the FM layer.

For some AFM materials (such as IrMn and FeMn), thermal treatment to induce a desired crystal structure is not required. However, a certain crystalline texture is still required. Therefore, an under layer is used to help grow the AFM layer in a desired texture. Reference 10 shows that if the IrMn layer does not grow in a (111) texture, there is no exchange coupling in between IrMn and NiFe. Table 2 shows the desired texture and annealing requirements for some AFM materials.

### **2.3.3 Composition**

In Hoshino's study<sup>(10)</sup>, the exchange coupling between NiFe and IrMn was found to depend on the composition of the IrMn alloy. The coupling depended on the grain size and crystal structure of the IrMn film. Figure 6<sup>(10)</sup> shows the  $H_{ua}$  vs. IrMn composition in the NiFe/IrMn system. In this study, x-ray diffraction analysis showed that for Ir compositions between 20 at.% and 41at.%, the (111) planes of FCC IrMn could be epitaxially grown on FCC NiFe (111) planes. In addition, the half width of the (111) IrMn peak shows that increasing Ir composition in this region can help grow larger grain size of the IrMn layer.

### **2.3.4 Thermal Stability**

Thermal stability of AFM materials can affect their pinning properties. Reference 19 and 20 report that the pinning fields of NiMn/NiFe, FeMn/NiFe, NiO/NiFe, IrMn/NiFe and IrMn/CoFe are temperature dependent. Figure 7<sup>(19)</sup> shows the normalized

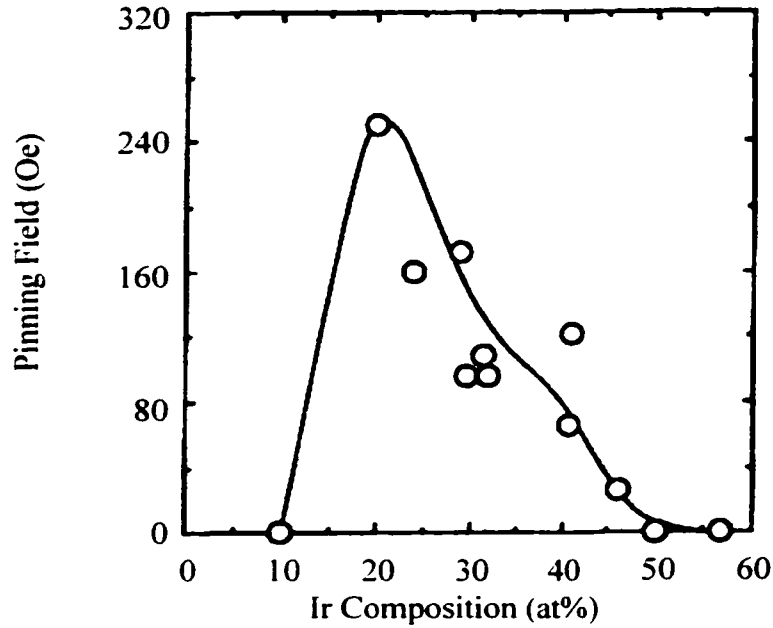


Figure 6. Dependence of  $H_{UA}$  on IrMn composition for Si/Zr/NiFe/IrMn/Zr<sup>(10)</sup>.

$H_{UA}$  ( $H_{UA, T^{\circ}C}/H_{UA, 27^{\circ}C}$ ) of different AFM/NiFe systems at different temperatures. From Figure 7, the pinning field decreases as temperature increases if IrMn, FeMn, and NiO are used. When the temperature reaches the blocking temperature, the exchange coupling disappears, and no pinning field exists. From this figure, the blocking temperature of FeMn and NiO are 150 and 200°C. Also, Figure 7 shows that the pinning field of NiMn/NiFe does not decrease as temperature increases.

## 2.4 Interlayer Coupling Field, $H_f$

Topics about interlayer coupling field are reviewed in References 4, 15, 22, 31, and 32. The interlayer coupling field is purely ferromagnetic. It is found that the interlayer coupling field is related to the spacer layer thickness. Magnetostatic interaction across the spacer layer is a model that explains this phenomenon. The spacer



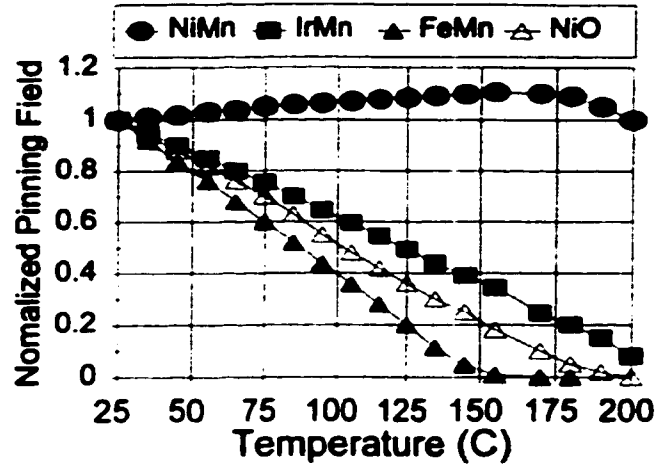


Figure 7. Normalized pinning fields vs. temperature for NiMn, FeMn, IrMn, and NiO spin-valves<sup>(19)</sup>.

layer thickness dependence has been explained as magnetostatic coupling. In the real world, thin film surfaces are rough. In spin-valves, two ferromagnetic layers are separated by a nonmagnetic spacer layer. The protrusions of the rough interface in the ferromagnetic layer will have magnetic poles on them, and a dipole field will be set up. If these protrusions occur in all three layers one above another, the dipole fields will interact with each other and tend to form a parallel alignment of the dipole fields. This effect is called “orange peel” coupling. Figure 8<sup>(31)</sup> shows the schematic view of this model. From this model, it is found that  $H_f$  can be described as a function of spacer layer thickness, as shown in Equation 3.

$$H_f \propto 1/\exp(\sqrt{t_{\text{spacer}}}) \quad (\text{Eq. 3})$$

where  $t_{\text{spacer}}$  is the thickness of the spacer layer.

The interfacial roughness in a spin-valve multilayer film can affect the interlayer coupling field and film resistance. Figure 8 shows as the slope of protrusions getting steeper and steeper, the magnetic pole density getting greater and greater. This means the

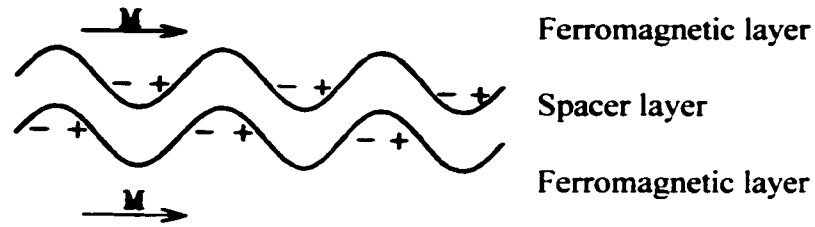


Figure 8. An illustration of the orange peel coupling in which magnetostatic coupling occurs due to the interaction of magnetic poles in a magnetic/nonmagnetic/magnetic structure with conformal roughness<sup>(31)</sup>.

stronger coupling. In addition, the closer the peaks and valleys of protrusions the stronger the interlayer coupling field. In order to decrease the interlayer coupling, a surfactant is used to smooth the interfacial roughness. Reference 7 and 8 studied the In, Pb, and Au as surfactant to decrease  $H_f$ .

## 2.5 Thin Film Resistance

The resistivity of a thin metal film is determined by three properties: intrinsic material properties, electron scattering in grain boundaries, and electron scattering at the surface. In spin-valve multilayer thin film applications, surface/interface scattering dominates the resistance of the film. It was found in Egelhoff's study<sup>(6)</sup> that the mean free path of the spin-valves was limited by diffuse electron scattering at the top and bottom surfaces. If electron scattering at the spin-valves can be made more specular, the resistance of the film can be reduced. The GMR ratio will, therefore, increase. Figure 9<sup>(6)</sup> shows a schematic view of specular electron scattering increase the mean free path of the single spin-valves. One way to increase the specular scattering and decrease the resistivity is to smooth the interface. In spin-valves, a surfactant is introduced to smooth

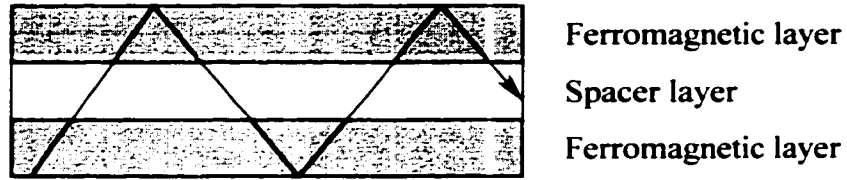


Figure 9. Illustration of specular electron scattering increase the electron mean free path<sup>(6)</sup>.

the roughness of the interface and improve the GMR ratio. Reference 6 shows that oxygen is an excellent surfactant to provide a flat interface for the spin-valves. Figure 10<sup>(6)</sup> shows a schematic of how oxygen provides a smooth interface for the spin-valves. Protrusions in a rough film surface have more surface area. When the film is exposed to oxygen, the protrusions are oxidized first and faster than the flat area. A flat interface is formed between the oxide and the metal region. This flat interface can provide better

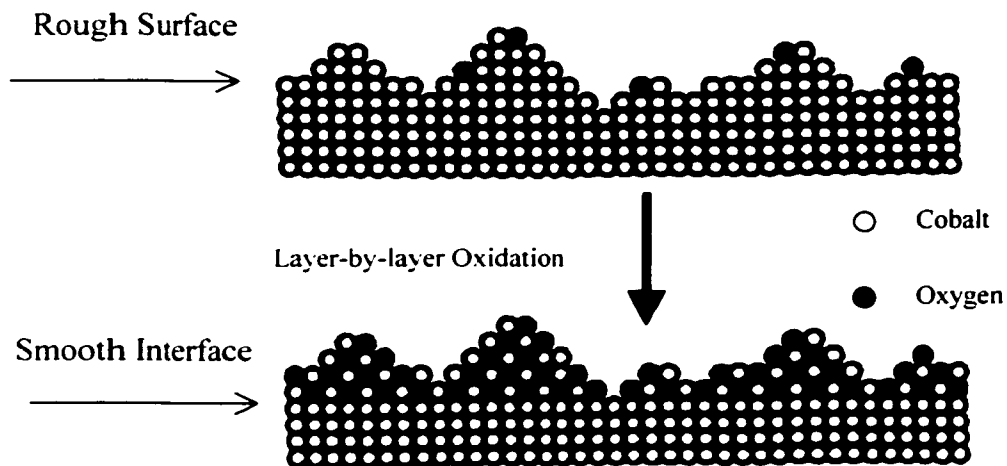


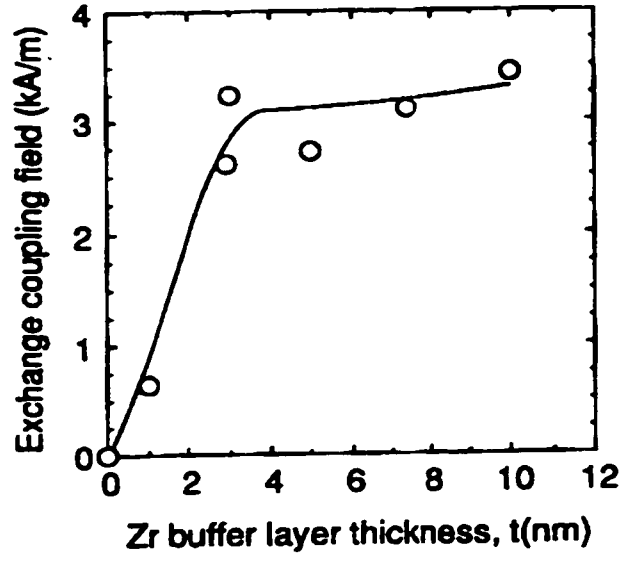
Figure 10. A schematic of how oxygen smoothing the interface of cobalt film<sup>(6)</sup>

specular electron scattering and can reduce the resistance of the film. Unfortunately, Reference 6 only used the oxygen to smooth the top of the spin-valve. There was no detailed information, such as oxygen exposure dosage, provided in this article. No other article was found that studied the oxygen surfactant. Therefore, studying the detailed effect of using oxygen as a surfactant is a new topic.

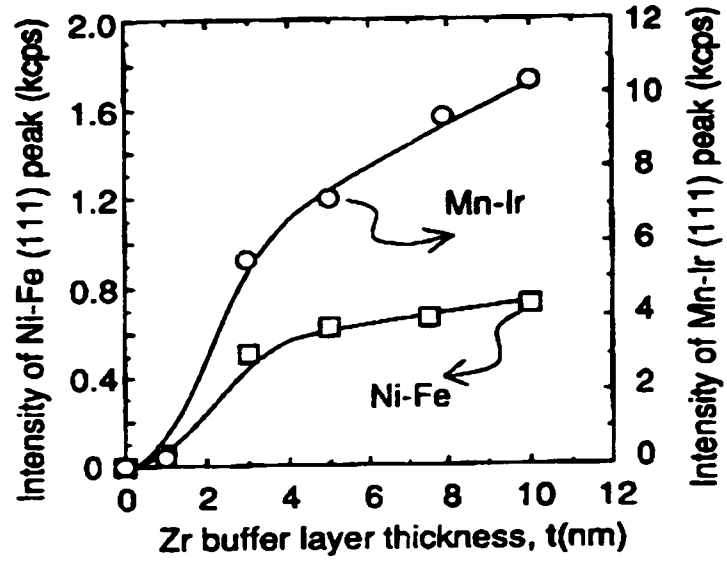
## **2.6 The Effects of Under Layer**

A under layer can facilitate growing the desired crystalline orientations and grain sizes of a spin-valve multilayer. References 9, 10, 11, and 33 report on the magnetic properties of spin valves with an under layer.

In order to provide good exchange coupling, AFM materials need to be grown in certain crystalline orientations. Al, Cu, Cr, Fe, Ta, and Zr have been evaluated as under layers for CoFe/Cu multilayers film in Gangopadhyay's study<sup>(11)</sup>. The study shows that different under layer materials can induce different Cu (111) peak intensities. These different intensities indicate how well the Cu film grew in the FCC (111) direction. Hoshino<sup>(10)</sup> deposited Zr, NiFe, and IrMn sequentially on top of a Si substrate. This study reports that the pinning field of the NiFe/IrMn bilayer without the Zr buffer layer is zero. When the thickness of Zr increases, both crystalline orientations of NiFe and IrMn films have strong (111) textures. The texture of IrMn induces more  $\gamma$ -Mn structure and provides better  $H_{UA}$ . Figure 11<sup>(10)</sup> shows the  $H_{UA}$  and X-ray diffraction (111) peak intensity vs. the thickness of Zr buffer layer.



(a)



(b)

Figure 11. (a)  $H_{UA}$  and (b) Intensity of (111) diffraction peaks vs. Zr layer thickness<sup>(10)</sup>

## 2.7 Thesis Orientation

From the literature review, it was believed that a study of a bottom spin-valve might reduce the complication of multilayer film deposition and provide insight into some of the properties of a dual spin-valve. However, a dual spin-valve is believed to possess a larger GMR ratio. Therefore, both bottom and dual spin-valves were studied.

To improve the interface, oxygen is believed to be a good surfactant to smooth the interface between layers. Because no detailed information about using oxygen as a surfactant is available, different oxygen exposure positions and dosages in bottom and dual spin-valves were studied.

For individual layer materials, Ta/Cu bilayer can be an under layer to induce the FCC (111) texture for IrMn. The IrMn/CoFe possesses large interfacial exchange coupling energy and good thermal stability. Cu is a common spacer layer material. Therefore, Ta/Cu bilayer was used as an under layer, IrMn was used as a pinning layer, and CoFe was used as a pinned and free layer.

## **Chapter 3**

### **Experimental Procedures**

#### **3.1 Experimental Plan**

The purpose of the experiments was to investigate the oxygen enhancement of the GMR effect in a CoFe/IrMn spin-valve. In order to achieve the best GMR effect, the composition of CoFe and the thickness of pinning, pinned, spacer, and free layer were optimized.

In order to analyze the magnetic properties of the samples, a B-H loop tracer was used to measure the interlayer coupling field and the GMR ratio, a vibrating sample magnetometer (VSM) was used to measure pinning field, and an in-line four-point probe was used to measure the sheet resistance.

Five experiments were done in this study. Experiments I and II investigated the oxygen effect in a single CoFe layer and in a multilayer of the [Ta/Cu/IrMn/CoFe/Cu] structure. Experiment III investigated the influence of spacer layer thickness. Experiment IV investigated the details of oxygen-enhanced IrMn-based bottom spin-valve. Experiment V investigated the oxygen-enhanced IrMn-based dual spin-valve.

The following sections discuss the details of the experimental procedures. Section 3.2 describes the sample preparation. Section 3.3 explains sample measurements. Section 3.4 through Section 3.8 explain the experiments.

## **3.2 Sample Preparation**

Sample preparation included three steps: substrate cleaning, thin film deposition, and annealing. These are described in the following paragraphs.

### **3.2.1 Substrate Cleaning**

In this study, the spin-valve sheet films were deposited on 25-mm-diameter glass substrates. Before the deposition, the substrates were cleaned by sulfuric acid etch and rinsed with deionized (DI) water. After the substrates were dried, they were stored in a dry tank for later use.

### **3.2.2 Thin Film Deposition**

The spin-valve films were deposited by DC magnetron sputtering. The system has the advantages of uniform deposition, low substrate temperature, high sputtering rate, and large area deposition.

Sputtering involves the acceleration of  $\text{Ar}^+$  ions that bombard a “target” or cathode. Through momentum transfer, the target surface material becomes volatile and is transported as vapor to the substrate. Figure 12 shows a schematic of the DC magnetron sputtering system that was used in this study.

The DC magnetron sputtering system was operated at ambient temperature and chamber base pressure of about  $9 \times 10^{-8}$  torr. A substrate holder that holds eight substrates was used in the system so that the substrates could be biased at 150 Oe during deposition. To ensure the uniform thickness of the deposited film, the holder was rotated with a rate of 30 rpm. The system that was used in the experiment has 4 sputtering guns. Four different targets, IrMn, Cu, Ta, and CoFe were mounted.  $\text{Ar}^+$  was introduced into the



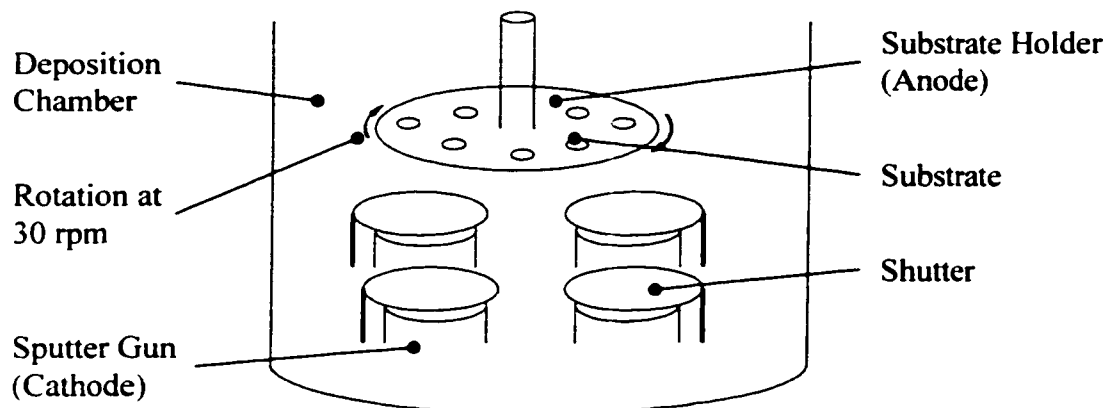


Figure 12. A schematic plot of DC magnetron sputtering system.

deposition chamber as a medium to initiate and maintain a glow discharge, and  $\text{Ar}^-$  pressure was controlled at 30 millitorr. The deposition rates were controlled by the power that was delivered to the target. The deposition rates of the IrMn, Cu, Ta, and CoFe were fixed at 0.7, 1.5, 1.1, and 1.4  $\text{\AA}/\text{sec}$ , respectively. Thickness control was done by controlling deposition time and monitored by quartz-crystal oscillator monitors.

Because oxygen was used as surfactant in this study, it was injected into the deposition chamber while on deposition break. For example, if the resistance of a single 40 $\text{\AA}$  CoFe with oxygen effect was to be studied, a 40 $\text{\AA}$  CoFe layer was deposited by two steps. The first deposition provided a certain thickness of CoFe, for example 20 $\text{\AA}$ . Next, a certain dosage of oxygen was introduced into the chamber to form an oxidation layer on the surface of CoFe. After that, the chamber pressure was pumped back to  $9 \times 10^{-8}$  torr. Once the pressure reached  $9 \times 10^{-8}$  torr, the other layer of CoFe (20 $\text{\AA}$  CoFe in this

example) was deposited above the oxide layer. The control of oxygen dosage was done by the oxygen flow rate and time. For example, a 1 c.c. oxygen dose can be injected into the chamber by flowing at 1sccm for 60 seconds.

### **3.2.3 Annealing**

After the sheet films were deposited, the samples were annealed. The purpose of annealing samples was to induce a magnetic anisotropy in the ferromagnetic layer(s) in the easy axis direction. It was found that substrates were not fully saturated during deposition. This caused the difficulty of magnetic properties measurements.

Annealing was done under vacuum at 200°C for 20 minutes and in a 500 Oe magnetic field. It took about two hours for the furnace to heat up from room temperature to 200°C, and about six hours to cool down from 200°C to room temperature.

## **3.3 Sample Measurement**

In order to understand the spin-valve properties, the multilayer films' magnetic properties and sheet resistance were measured. A vibrating sample magnetometer (VSM) and a B-H loop tracer were used to measure magnetic properties. The sample sheet resistance was measured by an in-line four-point probe.

### **3.3.1 VSM Measurement**

A common VSM measurement of the hysteresis loop of a single spin-valve is shown in Figure 13. In this figure, the horizontal axis is the applied magnetic field (H); the vertical axis is the magnetization (M). From the hysteresis loop, the magnetic properties of this measurement provide the pinning field ( $H_{UA}$ ), coercivity of the pinned layer ( $H_{cp}$ ), and saturation magnetization. This measurement has the advantage of a large

applied field, maximum field up to 10,000 Oe, and disadvantage of being slow, requiring about 14 minutes for a sample measurement. In addition, one step of applied magnetic field change is around 20 to 50 Oe. Therefore, this measurement cannot provide the magnetic properties that relate to the free layer, such as its coercivity.

### 3.3.2 B-H Loop Tracer Measurement

Magnetically soft materials are usually analyzed on a B-H loop tracer. The tracer

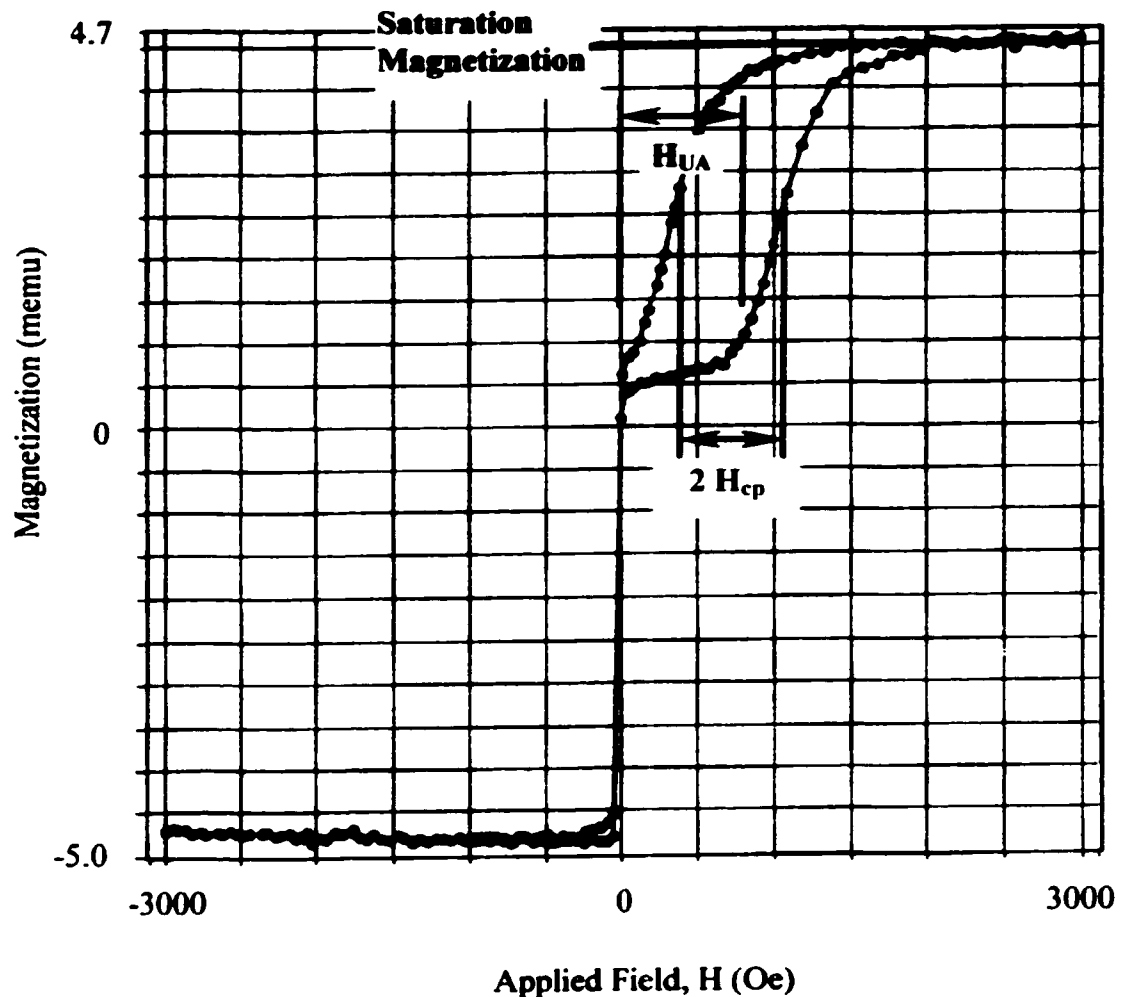


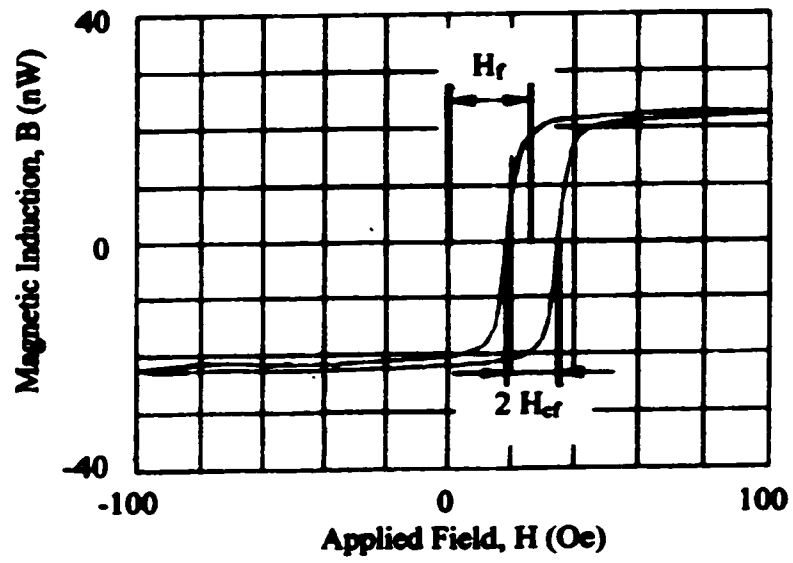
Figure 13. VSM measurement – hysteresis loop.

has the advantage of providing data quickly and the disadvantage of only a narrow range of applied magnetic field, between  $-100$  and  $100$  Oe. Figure 14(a) provides sample measurements of B-H loop tracer, where the vertical axis is magnetic induction (B) and the horizontal axis is the magnetic field (H). The magnetic properties that are provided by this measurement include interlayer coupling field ( $H_f$ ), coercivity of the free layer ( $H_{cf}$ ), and magnetic thickness of free layer. The shift of the magnetization curve along the applied field is the interlayer coupling field. The field required to reduce the magnetization to zero is the coercivity of free layer. The maximum magnetization in this measurement can be converted to the free layer thickness. Because the conversion from the magnetization to the layer thickness in this equipment is calibrated for NiFe, there is a factor of 1.5 difference for CoFe thickness. For example, if the measurement shows the magnetic thickness of CoFe free layer to be  $15\text{\AA}$ , the physical thickness of the CoFe free layer thickness is actually  $10\text{\AA}$ . In this written report, the reported CoFe thickness are all reported in magnetic thickness.

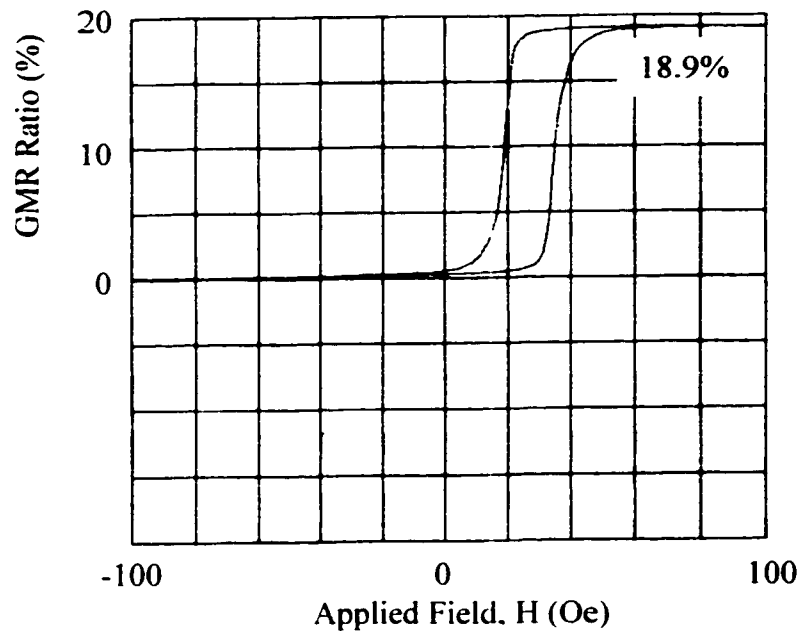
Figure 14(b) is the GMR ratio measurement. The GMR ratio is measured according to the Equation 1. When the applied field increases from zero to a saturation magnetic field, the film resistance changes from  $R_0$  to  $R[H_{\max}]$ . After converting to GMR ratio, the GMR ratio vs. the applied field is plotted out.

### **3.3.3 Sheet Resistance Measurement**

In this study, the sheet resistance of samples were measured by a conventional in-line 4-point probe. The unit of sheet resistance is  $\Omega/\text{sq}$ . The relation of sheet resistance to electrical resistance is shown in Equation 4.



(a)



(b)

Figure 14. (a) Magnetization curve of free layer measurement; (b) the GMR ratio measurement.

$$R_{\text{Sheet}} = 4.53 * R_{\text{Electrical}} \quad (\text{Eq. 4})$$

### 3.4 Experiment I

In Experiment I, a single layer of CoFe layer with and without oxygen effect was investigated. The purpose of Experiment I was to determine whether the oxygen affected the electrical property of the single CoFe layer. From the literature review<sup>(6)</sup>, we knew that a smooth interface formed by surfactant could reduce the surface scattering and could reduce the resistance of the spin-valve sheet film. However, whether this smooth interface could decrease the resistance of single CoFe layer was unknown. Therefore, a series of Co<sub>90</sub>Fe<sub>10</sub> single layer films with two different oxygen exposure dosages (0.5 sccm for 2 minutes and 1.0 sccm for 2 minutes) were studied. For comparison, a Co<sub>90</sub>Fe<sub>10</sub> single layer without oxygen exposure was also deposited. The single layer deposition was broken into two steps so that the oxygen could be introduced into the single layer, Figure 15. The first step of deposition deposited 30Å of Co<sub>90</sub>Fe<sub>10</sub>. Then, the 30Å Co<sub>90</sub>Fe<sub>10</sub> layer was exposed to different oxygen dosages (0.5 sccm and 1.0 sccm for 2 minutes). The second Co<sub>90</sub>Fe<sub>10</sub> with thickness  $t_{\text{CoFe}}$  was deposited after the exposure. The experimental matrix is shown in Table 3.

### 3.5 Experiment II

In Experiment II, a multilayer of substrate/Ta/Cu/IrMn/CoFe/Cu (Figure 16) with and without oxygen effect was investigated. The purpose of this experiment was threefold. The first one was to know whether the oxygen exposure could decrease the resistance of the multilayer, which might mean a smooth interface had formed. The second one was to know whether the exposure changed the pinning field. The third one

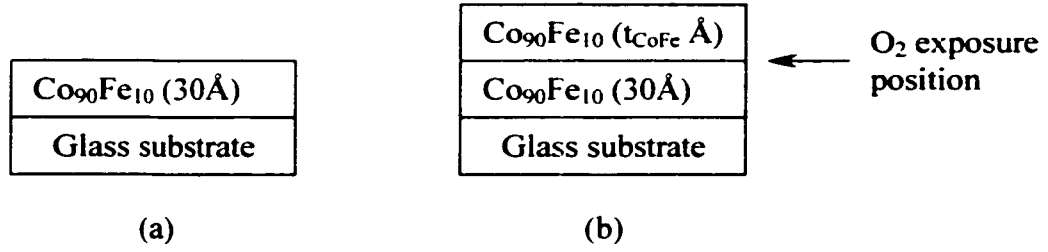


Figure 15. A schematic of CoFe single layer deposition; (a) the first step of CoFe deposition; (b) the second step of CoFe deposition.

Table 3. The experimental samples of Experiment I

Sample	0.5 sccm-2 min	Sample	1.0 sccm-2 min
EI-01	$t_{\text{CoFe}} = 75\text{A}$	EI-08	$t_{\text{CoFe}} = 75\text{A}$
EI-02	$t_{\text{CoFe}} = 68\text{A}$	EI-09	$t_{\text{CoFe}} = 68\text{A}$
EI-03	$t_{\text{CoFe}} = 60\text{A}$	EI-10	$t_{\text{CoFe}} = 60\text{A}$
EI-04	$t_{\text{CoFe}} = 53\text{A}$	EI-11	$t_{\text{CoFe}} = 53\text{A}$
EI-05	$t_{\text{CoFe}} = 45\text{A}$	EI-12	$t_{\text{CoFe}} = 45\text{A}$
EI-06	$t_{\text{CoFe}} = 38\text{A}$	EI-13	$t_{\text{CoFe}} = 38\text{A}$
EI-07	$t_{\text{CoFe}} = 30\text{A}$	EI-14	$t_{\text{CoFe}} = 30\text{A}$

was to know the best position to expose to oxygen. The film deposition was done sequentially from Ta (40Å), Cu (14Å), IrMn (70Å), Co<sub>90</sub>Fe<sub>10</sub> (45Å), and Cu (24Å). The deposition of 45Å Co<sub>90</sub>Fe<sub>10</sub> layer was done in two steps. The first time, a Co<sub>90</sub>Fe<sub>10</sub> thickness of  $d_{\text{II-CoFe}}$  Å was deposited (see Figure 16). This layer was then exposed to oxygen. Following, a  $(45-d_{\text{II-CoFe}})$  Å thickness of Co<sub>90</sub>Fe<sub>10</sub> was deposited. The oxygen dosage was 1.25 sccm for 2 minutes. The reason that Ta (40Å) and Cu (14Å) layers were deposited before the IrMn layer was to induce a desired IrMn texture, which was discussed in Section 2.3.2. Table 4 shows the experimental matrix.

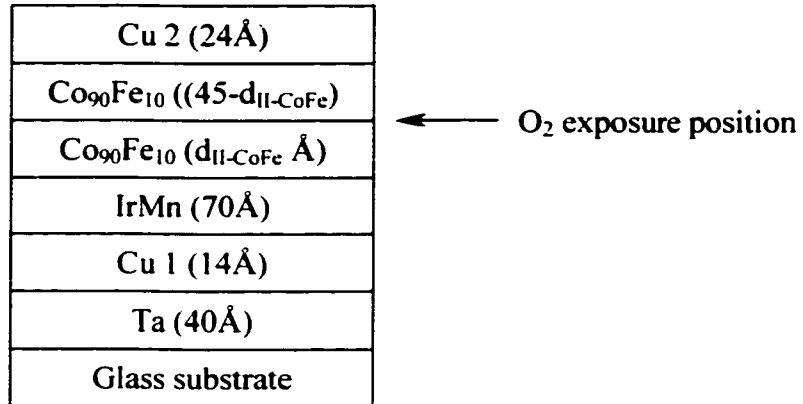


Figure 16. A schematic plot of multilayer structure in Experiment II.

Table 4. The experimental samples of Experiment II.

Sample with O <sub>2</sub> exposure	d <sub>II-CoFe</sub>	Sample without O <sub>2</sub> exposure
EII-01	14A	EII-08
EII-02	17A	
EII-03	21A	
EII-04	26A	
EII-05	31A	
EII-06	34A	
EII-07	38A	

### 3.6 Experiment III

In Experiment III, a bottom spin-valve with different Cu spacer layer thickness was investigated. The purpose of this experiment was to study whether the properties of the bottom spin-valve film changed if the Cu spacer layer thickness was changed and if the spin-valve was exposed to oxygen. The bottom spin-valve film in this study is shown in Figure 17. From the literature review<sup>(19, 29)</sup>, the spin-valve can be protected by



introducing a Ta over layer. Therefore, a Ta (35Å) over layer was deposited to protect the  $\text{Co}_{80}\text{Fe}_{20}$  from being oxidized in this experiment. The  $\text{Co}_{80}\text{Fe}_{20}$  free layer thickness was 45Å. The Cu spacer layer thickness was  $d_{\text{III-Cu}}$  Å. The deposition of  $\text{Co}_{80}\text{Fe}_{20}$  (45Å) pinned layer was done in two steps if this layer was exposed to oxygen. The oxygen exposure was introduced in the pinned layer and the dosage was 1.25 sccm for 2 minutes. An under layer, which was Ta (40Å)/Cu (14Å) bilayer, was deposited to help the IrMn (70Å) pinning layer to grow in a desired texture. The experimental matrix is shown in Table 5.

### **3.7 Experiment IV**

In Experiment IV, the bottom spin-valve with different oxygen exposure dosage and position was investigated. The purpose of this experiment was to study the detailed information, which included the oxygen exposure dosage and exposure position, of using oxygen as surfactant. The experiment deposited a bottom spin-valve sheet film, as shown in Figure 18. The  $\text{O}_2$  exposure dosages were 0.75 sccm, 1.25 sccm, and 1.50 sccm for 2 minutes, respectively. Different exposure positions were tried in the 45Å  $\text{Co}_{90}\text{Fe}_{10}$  pinned layer. The deposition of the pinned layer was done in two steps, as described above. Figure 18 shows the bottom spin-valve in this study. Table 6 shows the experimental matrix in Experiment IV.

### **3.8 Experiment V**

In Experiment V, a dual spin-valve structure, as shown in Figure 19, was investigated. The purpose of this experiment was to investigate the oxygen exposure position. The oxygen exposure positions that were studied included bottom pinned, top

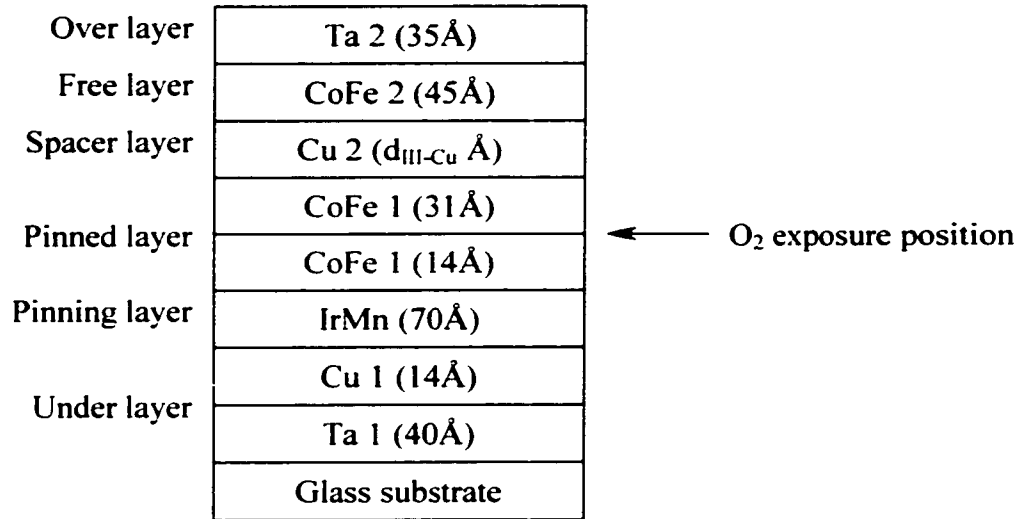


Figure 17. The bottom spin-valve structure in Experiment III.

Table 5. The experimental samples of Experiment III.

Without O <sub>2</sub> exposure		With O <sub>2</sub> exposure	
Sample	$d_{\text{III-Cu}}$	Sample	$d_{\text{III-Cu}}$
EIII-01	27	EIII-07	27
EIII-02	26	EIII-08	26
EIII-03	24	EIII-09	24
EIII-04	22	EIII-10	22
EIII-05	20	EIII-11	20
EIII-06	19	EIII-12	19

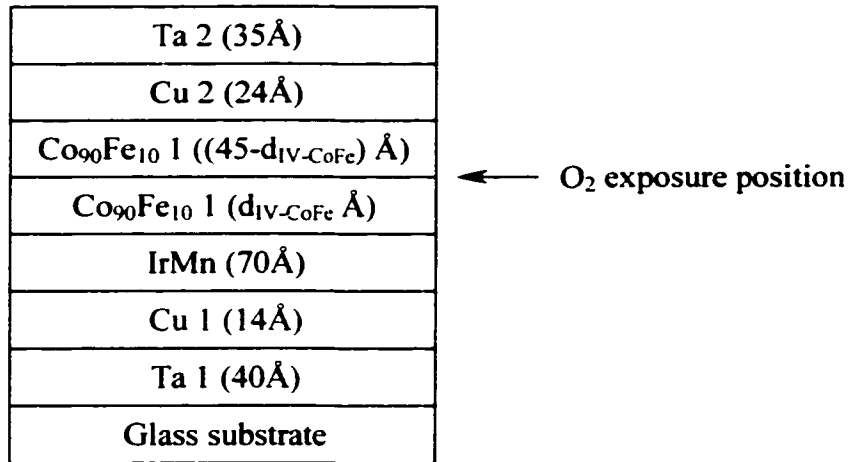


Figure 18. The bottom spin-valve structure in Experiment IV.

Table 6. The experimental samples of Experiment IV.

With O <sub>2</sub> exposure						No oxygen exposure
0.75 sccm-2 min		1.25 sccm-2 min		1.5 sccm-2 min		
Sample	d <sub>IV-CoFe</sub>	Sample	d <sub>IV-CoFe</sub>	Sample	d <sub>IV-CoFe</sub>	Sample
EIV-01	10	EIV-08	10	EIV-15	17	EIV-22
EIV-02	14	EIV-09	14	EIV-16	21	
EIV-03	17	EIV-10	17	EIV-17	24	
EIV-04	22	EIV-11	22	EIV-18	27	
EIV-05	27	EIV-12	27	EIV-19	31	
EIV-06	33	EIV-13	33	EIV-20	34	
EIV-07	38	EIV-14	38	EIV-21	38	

pinned, the bottom spacer, and the top spacer layers. The dual spin-valve structure in this study had the thickness of the Ta over layer 35Å, both the top and bottom IrMn pinning layers 70Å, both the top and bottom Co<sub>80</sub>Fe<sub>20</sub> pinned layers 45Å, the top spacer layer 27Å, the bottom spacer layer 24Å, and the Cu/Ta under layer 12 and 40Å. The first series of experiments tried to find the effect of oxygen exposure in bottom pinned layer (BP) and both bottom and top pinned layers (BP+TP). The exposure of oxygen on bottom pinned layer was similar to the exposure in Experiment II. The deposition of the top pinned layer was broken into two steps to allow the oxygen exposure. A thickness of  $d_{V-TP}$  Å was deposited in the first step followed by exposure to oxygen and then the second step deposition. The oxygen dosage used was 1.25 sccm for 2 minutes. The second series of experiments exposed the dual spin-valve to oxygen in three situations:

1. Bottom pinned layer and bottom spacer layer (BP+BS)
2. Bottom pinned layer and top spacer layer (BP+TS)
3. Bottom pinned layer, bottom spacer layer, and top spacer layer (BP+BS+TS)

The oxygen exposure position on bottom pinned layer, in this series, was 14Å above the top of bottom IrMn pinning layer. The exposure of the top/bottom spacer layer to oxygen was done right after the deposition of the top/bottom spacer layer. The oxygen exposure dosage was 1.25 sccm for 1.33 minutes. The experimental matrix is shown in Table 7.

### **3.9 Reproducibility of Samples**

In the Experiment I, II, and III, only one of each sample was deposited. In the Experiment IV and V, each sample was repeated three times in two separate deposition runs. Unfortunately, samples were easily broken. Some of the depositions had only two

identical samples left. The Experiment IV measurements on two nominally identical samples of GMR ratio, interlayer coupling field, and sheet resistance were within 1.2%, 2.4%, and 0.8%, respectively. The Experiment V measurements showed that the GMR ratio, interlayer coupling field, and sheet resistance were within 1.5%, 2.6%, and 0.6%, respectively, for two nominally identical samples.

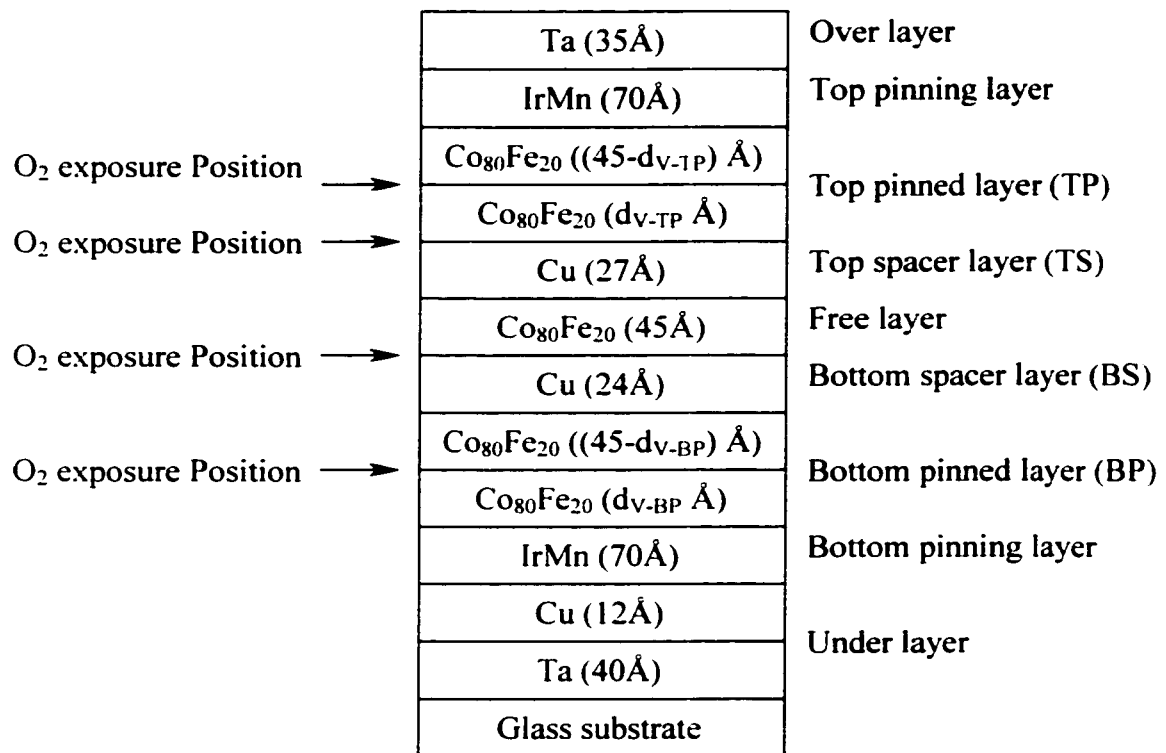


Figure 19. A schematic plot of dual spin-valve structure in Experiment V.

Table 7. The experimental plan of Experiment V.

O <sub>2</sub> exposure on BP only		O <sub>2</sub> exposure on both BP+TP			O <sub>2</sub> exposure position
Sample	d <sub>V-BP</sub>	Sample	d <sub>V-TP</sub>	Sample	
EV-01	14	EV-08	10	EV-15	BP+BS
EV-02	17	EV-09	14	EV-16	BP+TS
EV-03	21	EV-10	17	EV-17	BP+BS+TS
EV-04	26	EV-11	21		
EV-05	31	EV-12	26	Sample	No O <sub>2</sub> exposure
EV-06	34	EV-13	31	EV-18	
EV-07	38	EV-14	34		

## Chapter 4

### Results and Discussion

#### 4.1 The Effect of Oxygen Exposure on GMR Ratio

The experimental results suggest that GMR ratio will be increased with an optimal oxygen exposure dosage and position. Figures 20 and 21 show the GMR ratio in the bottom spin-valve. Figure 22 shows the GMR ratio in the dual spin-valve.

The results of the bottom spin-valve GMR ratio with different oxygen exposure dosage and pinned layer exposure position are shown in Figure 20. The  $\text{Co}_{90}\text{Fe}_{10}$  is used as the pinned and free ferromagnetic layer material in this experiment. The bottom spin-valve GMR ratio without oxygen-enhancement is 8.6%. The highest bottom spin-valve GMR ratio with oxygen enhancement is 13.1%. The optimal exposure dosage in this study is 1.25 sccm oxygen for 2 minutes. The optimal range of pinned layer exposure position ( $d_{\text{IV-Co-Fe}}$ ) is between 14 and 21 Å. The GMR ratio decreases significantly when the exposure position is above 30 Å.

The bottom spin-valve with exposure of 1.25 sccm oxygen for 120 seconds in different  $\text{Co}_{90}\text{Fe}_{10}$  pinned layer position suggests if the oxygen exposure position is too close to the pinned layer, the GMR ratio drops dramatically. A possible reason is that the interface between pinned and pinning field is oxidized. This oxidation layer separates the pinning and pinned layers. Therefore, the pinned layer no longer is pinned by the pinning layer, and the pinning field drops to zero or almost zero Oe. The pinning field of this spin-valve, shown in Figure 23, supports this assumption.

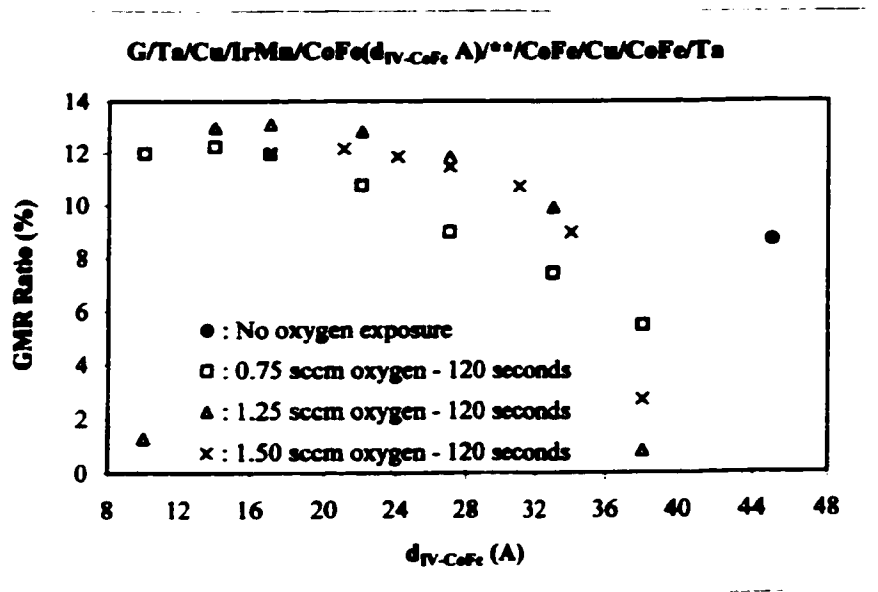


Figure 20. The GMR ratio of bottom spin-valve with different O<sub>2</sub> exposure positions and dosages: here, \*\* shows the O<sub>2</sub> exposure position. The total pinned layer thickness is 45Å.

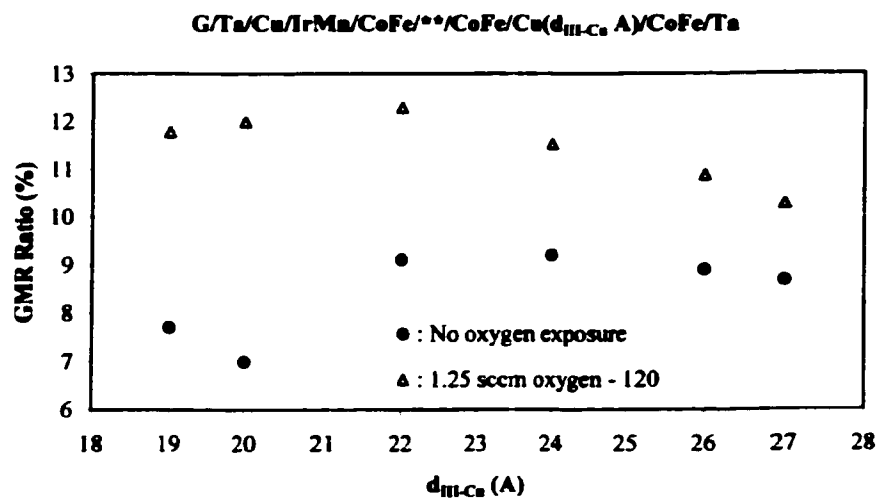


Figure 21. The GMR ratio of bottom spin-valve with different Cu spacer layer thickness: here, \*\* shows the O<sub>2</sub> exposure position. The total pinned layer thickness is 45Å.



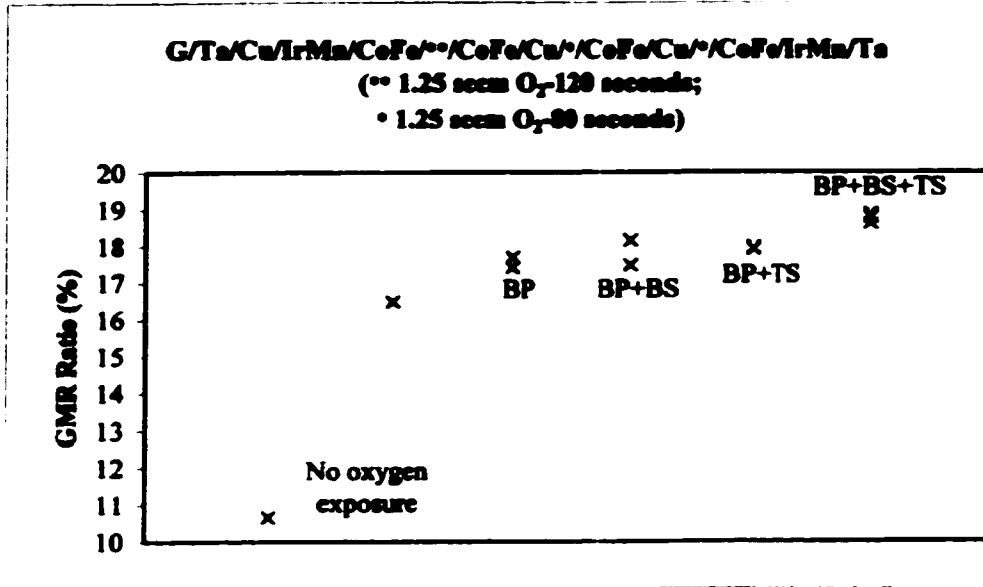


Figure 22. The GMR ratio of dual spin-valve with different oxygen exposure positions; here \*\* and \* show the oxygen exposure position.

The GMR ratio of bottom spin-valves with different Cu spacer layer thickness is shown in Figure 21. Co<sub>80</sub>Fe<sub>20</sub> was used as the pinned and free ferromagnetic layer material. The GMR effect of the bottom spin-valve is improved drastically by the exposure to oxygen. The highest GMR ratio is 12.3%. The highest GMR was found when the Cu spacer layer is between 20 and 24Å.

The results of the dual spin-valve GMR ratio with different oxygen exposure positions are shown in Figure 22. The highest GMR ratio in this experiment is 18.9% with oxygen exposure position on the bottom pinned, the bottom spacer, and top spacer layers. The oxygen dosage used in this sample was 1.25 sccm for 2 minutes in the

bottom pinned layer and 1.25 sccm for 1.33 minutes in both the bottom and top spacer layers.

## 4.2 The Effect of the Oxygen Exposure on Sheet Resistance

This section shows the sheet resistance of the oxygen exposure effect in three figures: Figure 24 (single CoFe layer), Figure 25 (multilayer structure), and Figure 26 (the bottom spin-valve structure).

Figure 24 shows the sheet resistance of the single  $\text{Co}_{90}\text{Fe}_{10}$  layer with and without oxygen exposure. The layer without oxygen exposure shows the lowest sheet resistance. A larger oxygen exposure dosage results in a larger sheet resistance of the single layer.

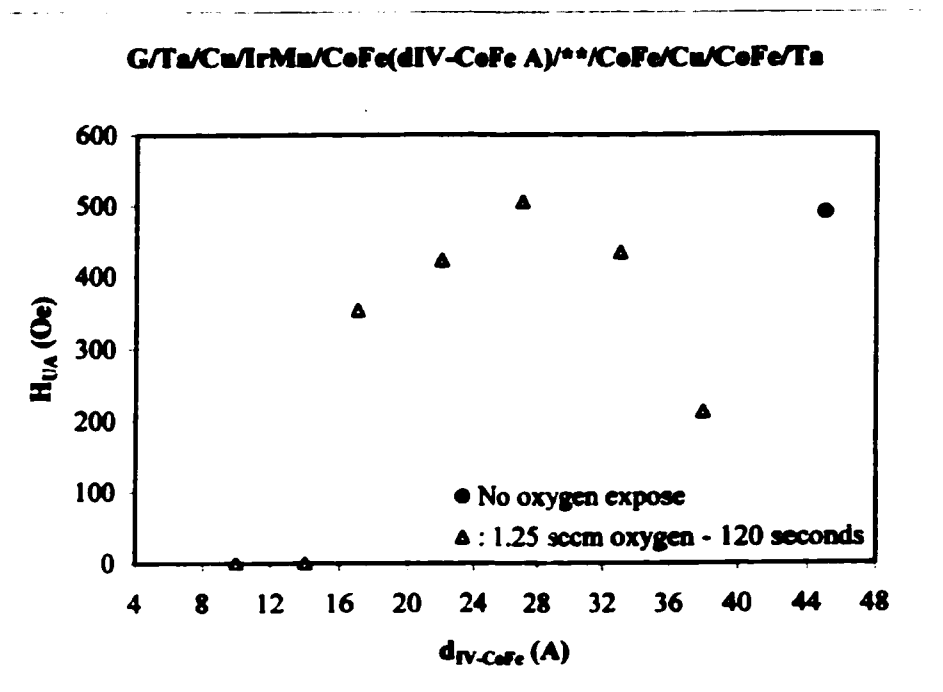


Figure 23. The pinning field of bottom spin-valve with oxygen exposure; here. \*\* shows the oxygen exposure position.

Figure 25 shows the sheet resistance of the multilayer structure. The structure is similar to the bottom spin-valve but without free and over layer. The sheet resistance of this structure also increases with oxygen exposure.

Figure 26 shows the sheet resistance of the bottom spin-valve structure with different O<sub>2</sub> exposure positions and dosages. The results show that the sheet resistance of the bottom spin-valve decreases with oxygen exposure. Thus, that the enhancement of the GMR ratio of the spin-valves is not due to a reduction in sheet resistance of the single layers, but rather depends on the composite multilayer spin-valve structure. The existence of the pinned layer-free layer interface appears to be necessary for the GMR enhancement.

### **4.3 The Effect of the Oxygen Exposure on Interlayer Coupling Field**

Figure 27 shows the effect of the oxygen exposure on the interlayer coupling field,  $H_f$ . The plot shows that the  $H_f$  can be reduced if oxygen exposure is introduced. There is one abnormally low interlayer coupling field point (4.7 Oe) in this figure. One possible explanation of this low  $H_f$  is that the pinned layer is no longer pinned by the pinning layer. Therefore, the magnetostatic interaction between pinned and free layer becomes small. This is an unwanted situation because of the low GMR ratio and zero  $H_{UA}$ . This was discussed in Section 4.1.

Figure 28 shows the  $H_f$  decreasing as the Cu spacer layer thickness of the bottom spin-valve is increasing. Figure 29 shows the  $H_f$  change as the oxygen exposure position changes. Detailed discussion of these two plots is given in the next section.

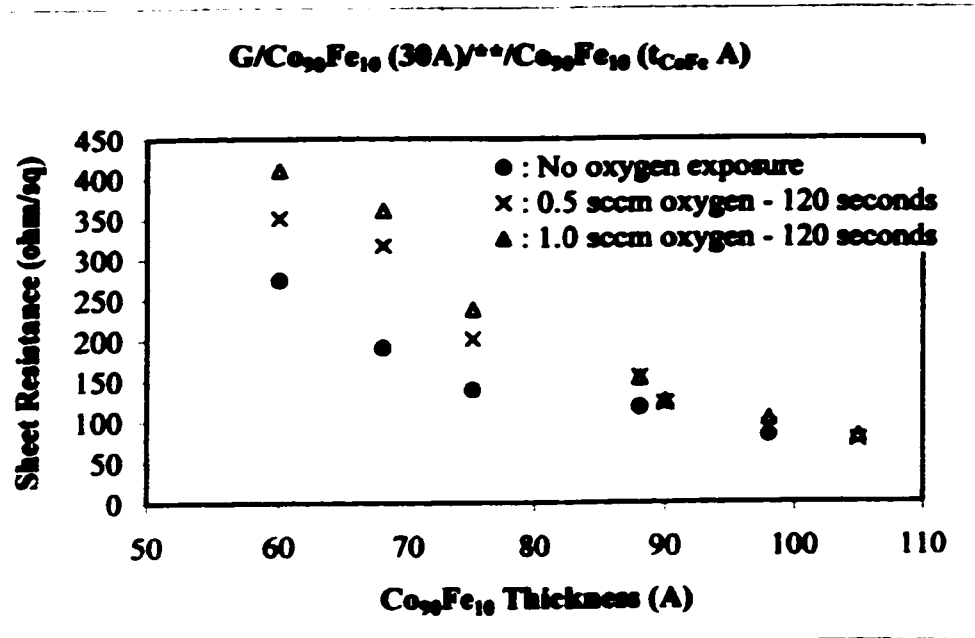


Figure 24. The sheet resistance of the single Co<sub>90</sub>Fe<sub>10</sub> layer with and without oxygen exposure; here, \*\* shows the oxygen exposure position.

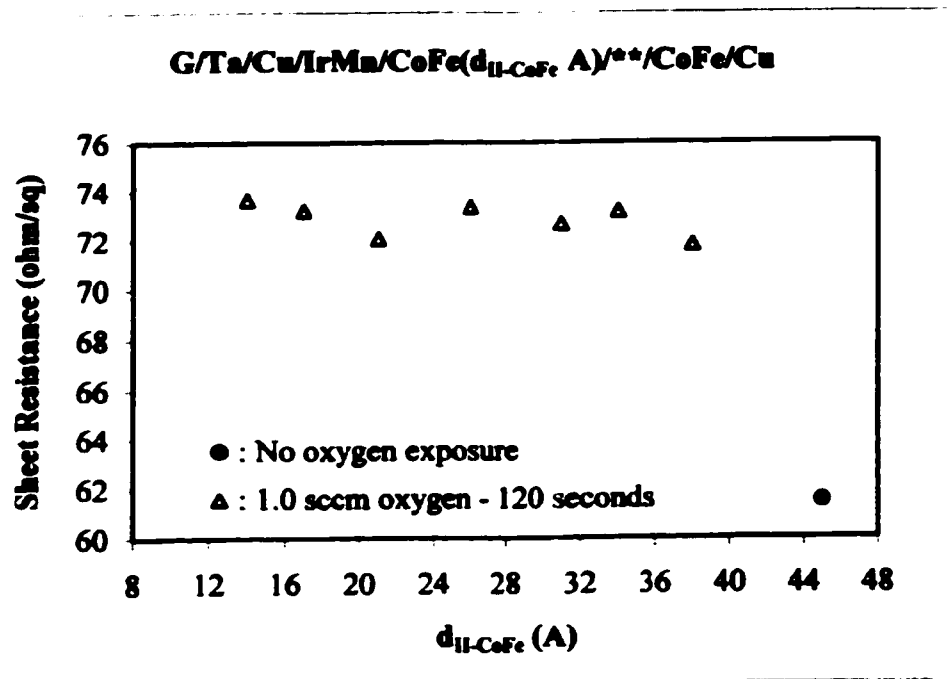


Figure 25. The sheet resistance of the multilayer structure; here, \*\* shows the oxygen exposure position.

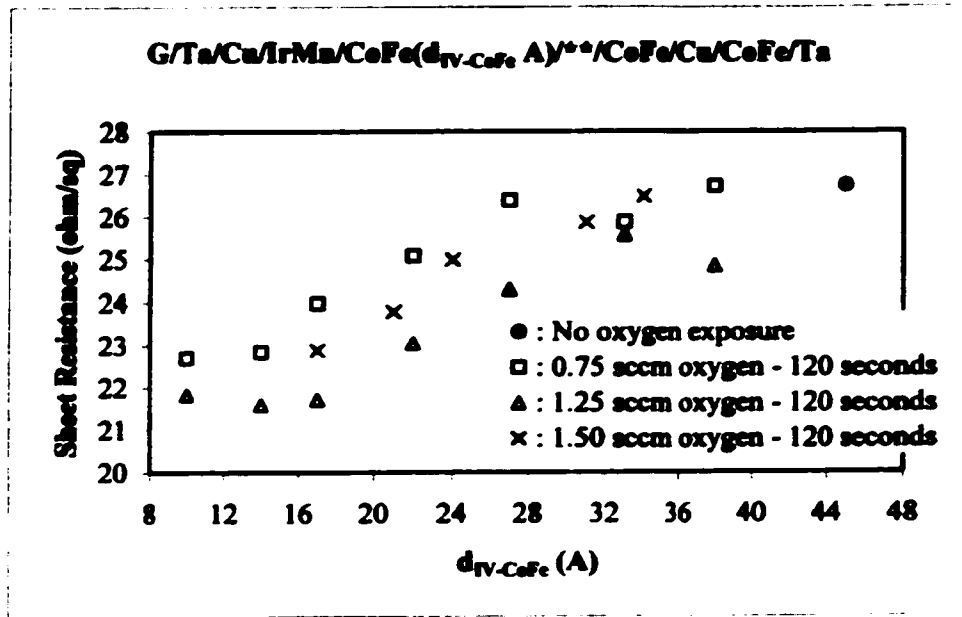


Figure 26. The sheet resistance of bottom spin-valve with different O<sub>2</sub> exposure positions and dosages; here, \*\* shows the O<sub>2</sub> exposure position.

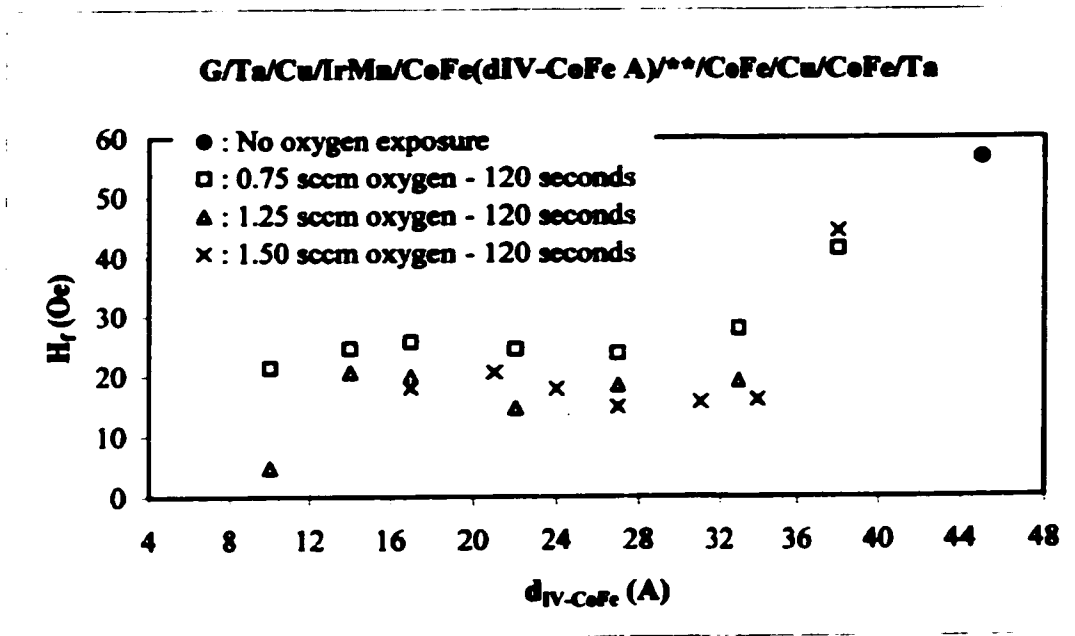


Figure 27. The effect of the oxygen exposure effect on interlayer coupling field. H<sub>I</sub>

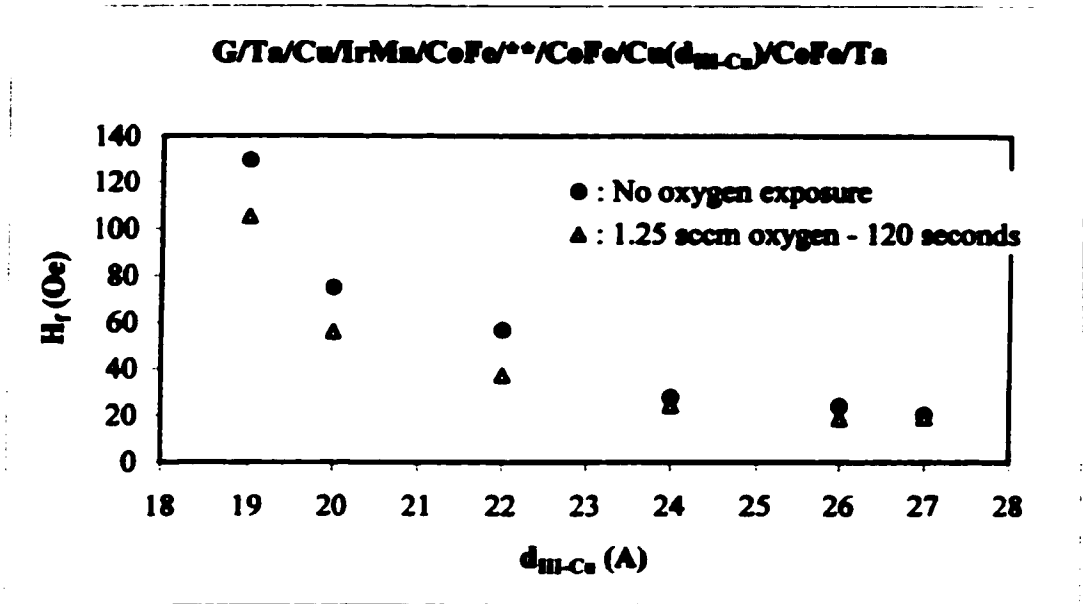


Figure 28. The  $H_f$  vs. the Cu spacer layer thickness; here, \*\* shows the oxygen exposure position.

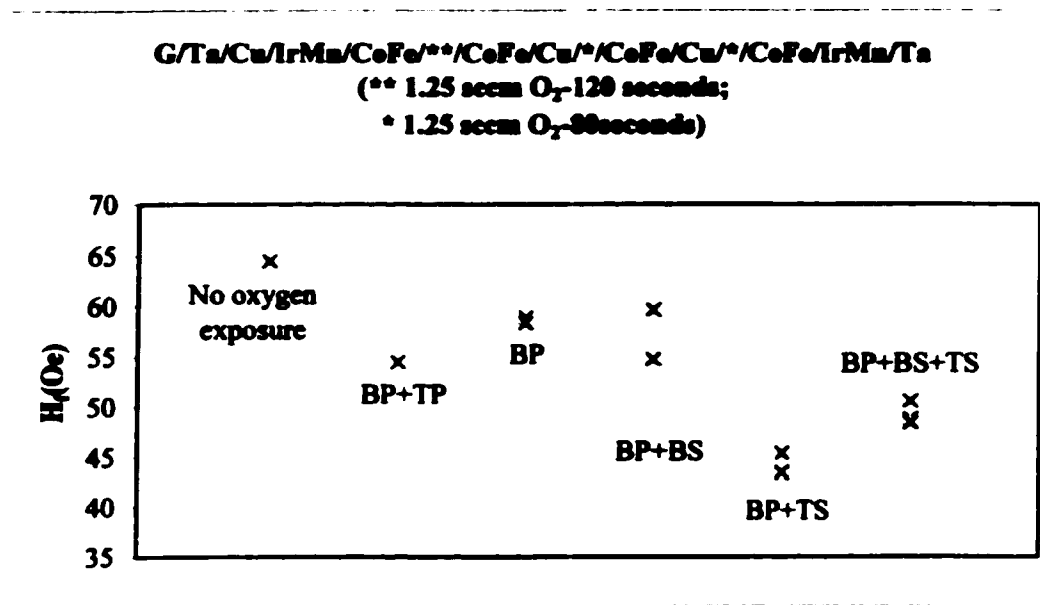


Figure 29. The  $H_f$  change with the different oxygen exposure positions in dual spin-valve; here, \*\* and \* show the oxygen exposure positions.

#### **4.4 Relationship Between Sheet Resistance and $H_f$**

This study shows that a decrease of the sheet resistance and the interlayer coupling field of the spin-valve occur with appropriate oxygen exposure dosage and position. The sheet resistance of the highest performance dual spin-valve is 12.9 and 13.8 ohm/sq with and without the oxygen exposure, respectively; the dual spin-valve GMR ratio is 18.9% and 10.7% with and without the oxygen exposure, respectively. According to the GMR ratio formula (Equation 1), if only the resistance change was considered, the GMR ratio would change from 10.7% to only 11.4%, which is a 6.5% increase, after the oxygen exposure. However, the result in this experiment shows a 76% increase in the GMR ratio. This indicates an enhancement of specular scattering. From previous work<sup>(6)</sup> we know if a proper surfactant is introduced, a smoother interface can be formed. This smooth interface for the spin-valve can decrease the sheet resistance and enhance the GMR ratio. Therefore, it is assumed a smooth interface as a result of oxygen exposure is formed in this oxygen study. This smooth interface enhances the specular scattering. Because of specular scattering, the electrical current is confined in the pinning, spacer, and pinned layers and does not experience shunting to other layers. Therefore, not only the sheet resistance of the dual spin-valve is reduced, but the GMR ratio is also enhanced.

In addition, the results of the interlayer coupling field of the dual spin-valve, shown in Figure 29, suggest a smooth interface, as a result of the oxygen exposure, in Cu spacer layer. As discussed in Section 2.4, the rougher the interface in the Cu spacer layer, the stronger the interlayer coupling field. The  $H_f$  with the oxygen exposure on

spacer layer is lower than the  $H_f$  without the oxygen exposure. Therefore, the smooth interface is assumed. Because the thickness of the top and bottom spacer layers (24 and 27Å, respectively) are different, the exposure results are different. Figure 28 shows that if the Cu spacer layer thickness is larger than 24Å, the  $H_f$  is not sensitive to the Cu spacer layer thickness. However, if the Cu layer thickness is smaller than 24Å, the  $H_f$  is sensitive to the Cu spacer layer thickness. When the spacer layer of the dual spin-valve is exposed to oxygen, the thickness of Cu layer decreases. Because the decreasing thickness of the bottom Cu spacer layer (24Å), as a result of the oxygen exposure, is in the thickness sensitive region, the reduction of the  $H_f$  is not as large as when the top spacer layer (27Å, which is not in the Cu layer sensitive region) is exposed to oxygen.

We have no direct evidence for whether a smooth interface was formed in this study; however, similar work<sup>(34)</sup> on ion beam sputtered samples indicates some evidence. The x-ray reflectivity data in that study<sup>(34)</sup> showed a smooth interface for the spin-valve with oxygen exposure. This smooth interface reduced the surface scattering and enhanced the specular scattering in the spin-valve. The result is a smaller sheet resistance in the spin-valve. In addition, the smooth interface in spin-valve causes a lower  $H_f$ . The combination of these two factors is believed to have caused the enhancement of the GMR ratio.

#### **4.5 Shift of Hysteresis Loop in Dual Spin-Valve**

As discussed in Section 2.3.1, the shift of the hysteresis loop is caused by the pinning field. The VSM measurement of a dual spin-valve, as shown in Figure 31, shows that the hysteresis loop is shifted twice. This phenomenon suggests that the bottom



pinning field ( $H_{UA}$  bottom) and top pinning field ( $H_{UA}$  top) in the dual spin-valve are different. In order to know more about the shifts, one sample (Figure 30) with different thickness of bottom and top pinned layers was deposited. The bottom and top pinned layer had the thickness of 55 and 37Å, respectively. Since the total magnetization of the pinned layer depends on its thickness, the magnetization of the bottom and top pinned layers were different. Figure 31 shows the VSM sample measurement of this sample. It is found that the bottom and top shift belongs to the bottom and top pinned layers, respectively. However, the cause of the different pinning field of the bottom and top pinning is unknown. Additional study, such as on interfacial roughness, grain size, and layer texture, is needed.

Ta (35Å)
Co <sub>80</sub> Fe <sub>20</sub> (37Å)
IrMn (59Å)
Cu (27Å)
Co <sub>80</sub> Fe <sub>20</sub> (45Å)
Cu (24Å)
Co <sub>80</sub> Fe <sub>20</sub> (55Å)
IrMn (59Å)
Cu (12Å)
Ta (40Å)
Glass substrate

Figure 30. The structure of different pinned layer thickness dual spin-valve.

memu

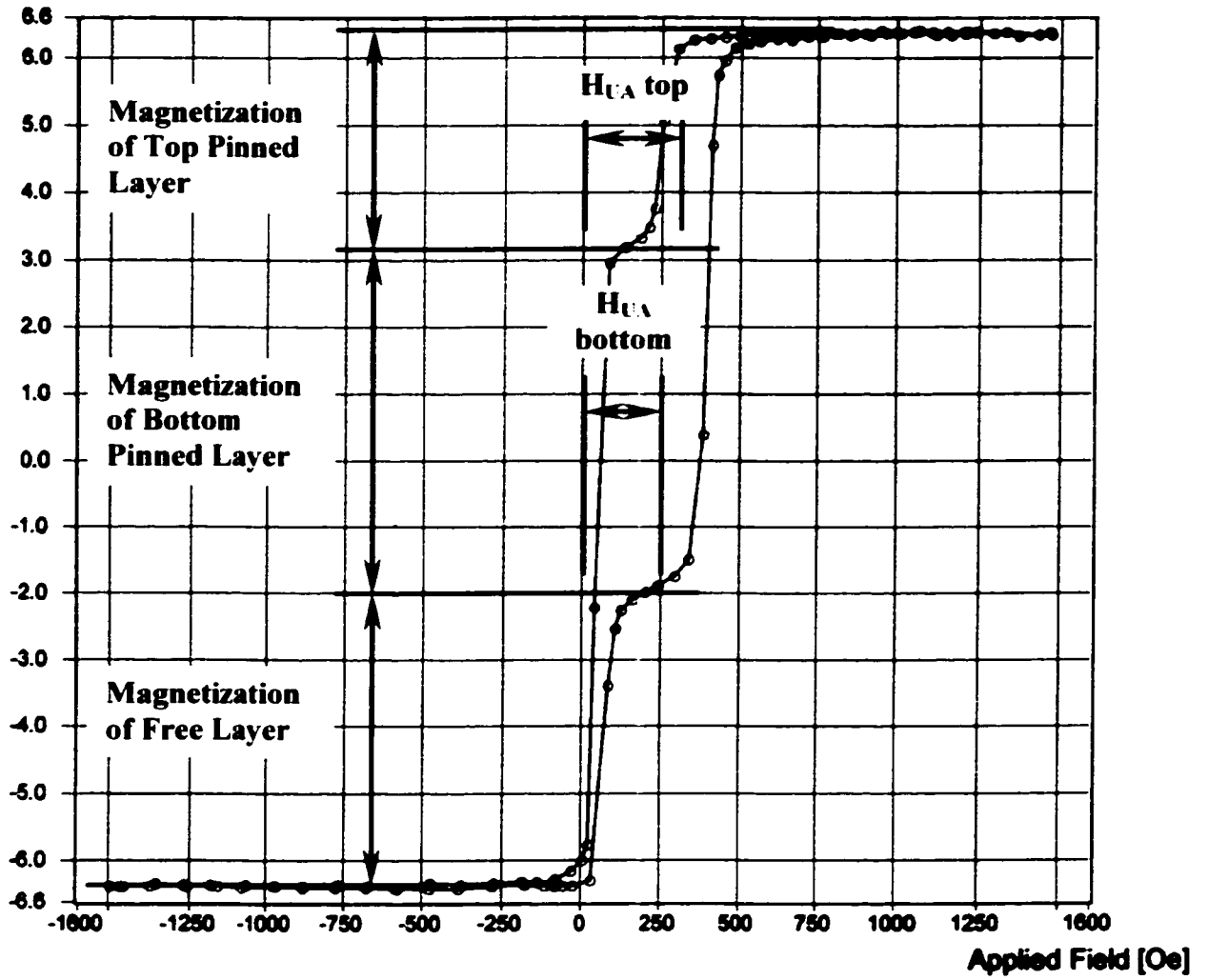


Figure 31. The VSM measurement of the different pinned layer thickness dual spin-valve.

## **Chapter 5**

### **Conclusions**

#### **5.1 Summary**

The oxygen effect on the performance of bottom and dual spin-valves was studied in this thesis. The experiments indicate that a smooth interface as a result of the oxygen exposure was formed. This smooth interface enhances the specular scattering. Consequently, the sheet resistance of the spin-valves decrease, and the GMR of the spin-valves increases. This study found the best exposure dosage (1.25 sccm oxygen for 2 minutes) and an optimal pinned layer exposure position ( $d_{IV-CoFe}$  between 14 and 21Å) for the bottom spin-valve. The best bottom spin-valve GMR ratio with oxygen-enhancement was 13.1%. The best oxygen exposure dosages (1.25 sccm oxygen for 2 minutes in the bottom pinned layer and 1.25 sccm oxygen for 1.33 minutes in the Cu spacer) and an optimal oxygen exposure positions (in bottom pinned, bottom spacer, and top spacer layers) in the dual spin-valve were also found. The best dual spin-valve GMR ratio was 18.9%.

In addition, the experiments indicate that the Cu spacer layer of the dual spin-valve exposed to oxygen forms a smooth interface and causes a decrease of the interlayer coupling field. Therefore, oxygen can be used as a surfactant in the GMR spin-valves to improve their properties.

## **5.2 Suggestions for Future Study**

Because of the complexity of the multilayer spin-valves, there still are many unknowns in this study. Some suggested topics are given here.

1. Study the thermal stability of the spin-valves. Because disk hard drives usually operate at about 100°C for a long time, atoms may diffuse between layers, causing a degradation of the magnetic performance.
2. Optimize the interlayer coupling field ( $H_f$ ) and the coercivity of free layer ( $H_{cf}$ ). The DC magnetron sputtering system used in this study only has four sputtering guns and only can deposit four materials. A NiFe target could not be installed and used as the material of free layer. Therefore, the coercivity of the free layer cannot be reduced to smaller than 5 Oe. In addition, if more materials, such as Co, can be sputtered and deposited as part of the free layer, the  $H_f$  may be reduced to smaller than 10 Oe.
3. Use X-ray diffraction or TEM to observe the microstructure of the layers, such as crystal structure, grain size, interface.
4. Optimize the deposition conditions, such as the base pressure and power of the sputtering system.

## References

1. M. N. Baibich, J. M. Broto, A. Fert, F. Nguyen Van Dau, F. Petroff, P. Eitenne, G. Creuzet, A. Friederich, and J. Chazelas, *Phys. Rev. Lett.* **61** (21), 2472 (1988).
2. B. Dieny, V. S. Speriosu, S. S. P. Parkin, B. A. Gurney, D. R. Wilhoit, and D. Mauri, *Phys. Rev. B*, **43** (1), 1297 (1991).
3. Kanu G. Ashar, *Magnetic Disk Drive Technology*, IEEE, **38**, (1997).
4. J. Kools, *IEEE Trans. on Magn.* **32** (4), 3165 (1996).
5. J. Kools and W. Kula, *J. Appl. Phys.* **85** (8), 4466 (1999).
6. W. Egelhoff, Jr., P. Chen, C. Powell, D. Parks, G. Serpa, and R. McMichael, *J. Vac. Sci. Technol. B*, **17** (4), 1702 (1999).
7. W. Egelhoff, Jr. P. Chen, C. Powell, M. Stiles, and R. McMichael, *J. Appl. Phys.* **79** (5), 2491 (1996).
8. W. Egelhoff, Jr. P. Chen, C. Powell, M. Stiles, and R. McMichael, *J. Appl. Phys.* **80** (9), 5183 (1996).
9. M. Pakala, Y. Huai, G. Anderson, and L. Miloslacsky, *J. Appl. Phys.* **87** (9), 6653 (2000).
10. K. Hoshino, R. Nakatani, H. Hoshiya, Y. Sugita, and S. Tsunashima, *Jpn. J. Appl. Phys.* **35**, 607 (1996).
11. S. Gangopadhyay, J. Shen, M. Kief, J. Barnard, and M. Parker, *IEEE Trans. Magn.* **31** (6), 3933 (1995).
12. D. Wang, J. Daughton, and C. Smith, *IEEE Trans. on Magn.*, **32** (5), 4728 (1996).
13. R. L. White, *IEEE Trans. on Magn.*, **28** (5), 2482 (1992).
14. K. Inomata, *J. Electroceramics*, 283 (1998).
15. W. F. Egelhoff, Jr., P. J. Chen, C. J. Powell, M. D. Stiles, and R. D. McMichael, *J. Appl. Phys.* **79** (8), 5277 (1996).
16. W. F. Egelhoff, Jr., T. Ha, R. D. K. Misra, Y. Kadmon, J. Nir, C. J. Powell, M. D. Stiles, and R. D. McMichael, *J. Appl. Phys.* **78** (1), 273 (1995).

17. Z. Oian and J. M. Sivertsen, *J. Appl. Phys.* **83** (11), 6825 (1998).
18. H. Sang and Y. W. Du, *J. Appl. Phys.* **85**(8), 4931 (1999).
19. S. Mao, N. Amin, and E. Murdock, *J. Appl. Phys.* **83** (11), 6807 (1998).
20. J. Driel, R. Coehoorn, K. Lenssen, A. Kuiper, and F. de Boer, *J. Appl. Phys.* **85** (8), 5522 (1999).
21. H. Fuke, K. Saito, Y. Kamiguchi, H. Iwasaki, and M. Sahashi, *J. Appl. Phys.* **81** (8), 4004 (1997).
22. T. Rijks, R. Coehoorn, J. Daemen, and W. de Jonge, *J. Appl. Phys.* **76** (2), 1092 (1994).
23. A. Devasahayam, P. Sides, and M. Kryder, *J. Appl. Phys.* **83** (11), 7216 (1998).
24. Y. Hamakawa, M. Komuro, K. Watanabe, H. Hoshiya, T. Okada, K. Nakamoto, Y. Suzuki, M. Fuyama, and H. Fukui, *IEEE Trans. Magn.*, **35** (2), 677 (1999).
25. R. Nakatani, H. Hoshiya, K. Hoshino, and Y. Sugita, *Jpn. J. Appl. Phys.: Part I.* **38** (4A), 1955 (1999).
26. S. Soeya, T. Imagawa, K. Mitsuoka, and S. Narishige, *J. Appl. Phys.* **76** (9), 5356 (1994).
27. T. Lin, C. Tsang, R. Fontana, and J. Howard, *IEEE Trans. Magn.* **31** (6), 2585 (1995).
28. H. Iwasaki, A. Saito, A. Tsutai, and M. Sahashi, *IEEE Trans. Magn.* **33** (5), 2875 (1995).
29. S. Cheng and P. Lubitz, *J. Appl. Phys.* **87** (9), 4927 (2000).
30. T. Umemoto, A. Maeda, S. Takahasi, T. Tanuma, and M. Kume, *Jpn. J. Appl. Phys.: Part I.* **36** (11), 6746 (1997).
31. W. Egelhoff, Jr., P. J. Chen, R. Misra, T. Ha, Y. Kadmon, C. Powell, M. Stiles, and R. McMichael, *J. Appl. Phys.* **79** (1), 282 (1996).
32. K. Hoshino, S. Noguchi, R. Nakatani, H. Hoshiya, and Y. Sugita, *Jpn. J. Appl. Phys.: Part I.* **33** (3A), 1327 (1994).

33. G. Choe and S. Gupta, IEEE Trans. Magn., **33** (5), 3691 (1997).

34. W. Y. Lee, H. C. Chang, D. Mauri, M. Toney, and P. Rice, to be published.